

Electronic Supplementary Information (ESI) for
Translucent Perovskite Photovoltaics for Building Integration

**D. B. Ritzer^{1*}, B. Abdollahi Nejand², M. A. Preciado-Ruiz², S. Gharibzadeh², H. Hu², A. Diercks²,
T. Feeney², B. S. Richards^{1,2}, T. Abzieher^{2†} and U. W. Paetzold^{1,2*}**

¹Institute of Microstructure Technology, Karlsruhe Institute of Technology, 76344 Eggenstein-Leopoldshafen, Germany

²Light Technology Institute, Karlsruhe Institute of Technology, 76131 Karlsruhe, Germany

*corresponding authors: David.Ritzer@kit.edu, Ulrich.Paetzold@kit.edu

†present address: National Renewable Energy Laboratory, Golden, CO 80401, United States

Experimental Procedures

Substrates:

All photovoltaic devices were fabricated in superstrate configuration. Polished soda-lime glass substrates of 1.1 mm thickness were either purchased with indium tin oxide coating (ITO, Luminescence Technology, CAS: 50926-11-9) or coated with a 230 nm IO:H front electrode. For single-junction solar cell fabrication, 16×16 mm² substrates with pre-patterned ITO were utilized while for submodule fabrication, 30×30 mm² substrates with unpatterned ITO were laser scribed as discussed below. 2-terminal perovskite-perovskite tandem solar cells and modules were fabricated on the IO:H coated glass substrates.

Single-junction perovskite solar cell fabrication:

Materials, solution precursors and solvents: 2PACz (TCI, CAS: 20999-38-6), Lead iodide (PbI_2 , TCI, CAS: 10101-63-0) and Lead Bromide ($PbBr_2$, TCI, CAS: 10031-22-8), Formamidinium iodide (FAI, Dyanamo, CAS: 879643-71-7), Methylammonium Bromide (MABr, Greatcell Solar, CAS: 6876-37-5), Cesium Iodide (CsI, abcr, CAS: 7789-17-5), Fullerene-C₆₀ (C₆₀, Sigma-Aldrich, CAS: 99685-96-8) and Bathocuproine (BCP, Lumescence Technology, CAS: 4733-39-5). Solvents including N,N-dimethylformamide ≥99.9% (DMF, anhydrous, 99.8%, CAS: 68-12-2), Dimethyl Sulfoxide anhydrous ≥99.9% (DMSO, CAS: 67-68-5), and Ethyl Acetate anhydrous 99.8% (EA, CAS: 141-78-6) were ordered from Sigma-Aldrich. Ethanol absolute 99.8% was ordered from VWR Chemicals.

Layer fabrication: ITO substrates (sheet resistance 15 Ω/sq, Luminescence Technology, CAS: 50926-11-9) were cleaned with acetone and isopropanol in an ultrasonic bath for 10 min each. The substrates were further treated with oxygen plasma for 3 min. As HTL, 2PACz (TCI, CAS: 20999-38-6) was deposited on the ITO substrates by spin-coating at 3000 r.p.m. for 30 s and was subsequently annealed at 100 °C for 10 min. The 2PACz solution was prepared by dissolving 2PACz in anhydrous ethanol with a concentration of 1 mM. The prepared solution was put in an ultrasonic bath for 20 min before it was used. The perovskite precursor solution was prepared by mixing PbI_2 (1.3 M), $PbBr_2$ (0.14 M), CsI (0.07 M), MABr (0.14 M) and FAI (1.2 M) in a mixture of DMF:DMSO (4:1). The perovskite films were spin-coated on the substrates at 1000 r.p.m. (200 r.p.m. s⁻¹) for 10 s and 5000 r.p.m. (2000 r.p.m. s⁻¹) for 30 s. 15-20 s after the start of the second step, ethyl acetate (150 μL) was casted at the center of the spinning substrate. The samples were then annealed at 100 °C for 45-60 min in nitrogen atmosphere. The absorber deposition was optimized to achieve a layer thickness of 600 nm. As the electron transport layer, 25 nm of C₆₀ and 7 nm BCP, were thermally evaporated at a rate of 0.1-0.2 Å s⁻¹ while maintaining a maximum pressure of 10⁻⁶ mbar. Finally, 75 nm of Au were thermally evaporated using a shadow mask with an active area of 10.5 mm² to complete the perovskite solar cells with 4 pixels per substrate.

Single-junction perovskite solar module fabrication:

Materials, solution precursors and solvents: 2PACz (TCI, CAS: 20999-38-6), Formamidinium iodide (FAI, Dyanamo, CAS: 879643-71-7), Cesium Iodide (CsI, abcr, CAS: 7789-17-5), Lead iodide (PbI_2 , TCI, CAS: 10101-63-0), Lead Bromide ($PbBr_2$, TCI, CAS: 10031-22-8), Lead Chloride ($PbCl_2$, TCI, CAS: 7758-95-4), Methylammonium Chloride (MACl, Dyanamo, CAS: 593-51-1), Lithium Fluoride (LiF, Sigma-Aldrich, CAS: 7789-24-4), Fullerene-C₆₀ (C₆₀, Sigma-Aldrich, CAS: 99685-96-8), Bathocuproine (BCP, Lumescence Technology, CAS: 4733-39-5). Solvents including N,N-dimethylformamide ≥99.9% (DMF, anhydrous, 99.8%, CAS: 68-12-2), Dimethyl Sulfoxide anhydrous ≥99.9%, Ethyl Acetate anhydrous 99.8%, Chlorobenzene anhydrous 99.8% (CB, CAS: 108-90-7) and Ethanol absolute 99.8% were ordered from Sigma-Aldrich.

Layer fabrication: The perovskite submodules with the layer stack glass/ITO/2PACz/Cs_{0.17}FA_{0.83}Pb(I_{0.92}Br_{0.08})₃/LiF/C₆₀/BCP/Au were fabricated following the device fabrication process described below. Glass substrates with 120 nm thick ITO coating (sheet resistance 15 Ω □, Luminescence Technology) and laser scribed P1 lines were cleaned for 10 min in an ultrasonic bath with deionized (DI) water, acetone, and isopropanol, followed by 3 min treatment with oxygen plasma. A thin 2PACz HTL prepared by dissolving 2PACz powder in anhydrous Ethanol at a concentration of 1 mmol l⁻¹ was deposited on the ITO substrate by spin-coating at 3000 r.p.m. for 30 s, followed by an annealing step at 100 °C for 10 min. The precursor solution of the double-cation Cs_{0.17}FA_{0.83}Pb(I_{0.92}Br_{0.08})₃ perovskite absorber layer was prepared by dissolving 0.83 mmol FAI (143 mg), 0.17 mmol CsI (44 mg), 0.88 mmol PbI_2 (444 mg, 10% excess of PbI_2), and 0.12 mmol $PbBr_2$ (46 mg) in a 1 mL solvent mixture of DMF:DMSO 4:1 volume ratio. Afterward, as a bulk passivation additive, 35 μL of $PbCl_2$:MACl solution with a molar ratio of 1:1 dissolved in 1 mL DMSO was added to the reference perovskite precursor solution. The solution was deposited on top of the HTL by a two-step spin coating process: i) 1000 r.p.m. (acceleration 2000 r.p.m. s⁻¹) for 10 s, ii) 5000 r.p.m. (acceleration 2000 r.p.m. s⁻¹) for 40 s. 150 μL CB was poured on the spinning substrate 20 s before the end of the second step. The samples were annealed at 100 °C for 30 min in an inert atmosphere. After the annealing step was finished, 1 nm lithium fluoride (LiF), 23 nm C₆₀ (Sigma) and 3 nm bathocuproine (BCP, Lumescence Technology) were thermally evaporated with an evaporation rate of 0.1-2 Å s⁻¹ at a pressure of 10⁻⁶ mbar. After laser scribing the P2 lines, a 75 nm thick gold layer was deposited via thermal evaporation. Last, the P3 line was laser scribed. All utilized laser scribing parameters followed the ones described below.

2-terminal perovskite-perovskite tandem solar cells and modules:

Materials, solution precursors and solvents: Formamidinium Iodide (FAI, GreatCell, CAS: 1415238-77-5), Methylammonium Iodide (MAI, GreatCell, CAS: 14965-49-2), Tin Iodide (SnI₂, Sigma-Aldrich, 99.999%, CAS: 7790-47-8), Lead Iodide (PbI_2 , Alfa Aesar, 99.999%, CAS: 10101-63-0), Lead Thiocyanate ($Pb(SCN)_2$, Sigma-Aldrich, 99.5%, CAS: 592-87-0), Tin Fluoride (SnF₂, Sigma-Aldrich, 99%, CAS: 7783-47-3), FABr, CsBr (Alfa Aesar), Lead Bromide ($PbBr_2$, TCI, CAS: 10031-22-8), PEDOT:PSS dispersion (Ossila, AI 4083, CAS: 155090-83-8) and Poly(bis(4-phenyl)(2,4,6-trimethylphenyl)amine (PTAA, 2 mg ml⁻¹ in toluene, CAS: 1333317-99-9). Solvents including N,N-

dimethylformamide (DMF, anhydrous, 99.8%, CAS: 68-12-2), Dimethyl Sulfoxide (DMSO, anhydrous, ≥99.9%, CAS: 67-68-5) and Ethyl Acetate (CAS: 141-78-6) were ordered from Sigma-Aldrich.

Layer fabrication: The fabrication followed the recipes described in our previous work.¹ Glass substrates coated with a 230 nm thick ITO:H front electrode were cleaned in deionized water, acetone and isopropanol in an ultrasonic bath for 10 min, respectively. Immediately before layer fabrication, the substrates were treated with oxygen plasma for 3 min. For HTL deposition, 70 µl of 2PACz solution in ethanol was spin coated at 3000 r.p.m. for 30 s and annealed at 100 °C for 10 min. Subsequently, the wide band gap perovskite was deposited in a glovebox with inert atmosphere. The 1 M precursor solution was prepared by mixing 82.5 mg FAI, 40 mg FABr, 31.1 mg CsI, 17 mg CsBr, 276.6 mg PbI₂ and 146.8 mg PbBr₂ in 4:1 DMF:DMSO and deposited via 2-step spin coating at 1000 r.p.m. for 10 s (2000 r.p.m. s⁻¹) and at 6000 r.p.m. for 30 s (2000 r.p.m. s⁻¹). 19 s before the end of the deposition process, 150 µl ethyl acetate was casted onto the wet film as antisolvent. The samples were annealed at 150 °C for 20 minutes. Afterwards, a 1 nm thick lithium fluoride (LiF, Sigma-Aldrich, CAS: 7789-24-4) thin film as well as a 15 nm thick layer of fullerene (C_{60} , Sigma-Aldrich, CAS: 99685-96-8) was thermally evaporated (OPTIvap, CreaPhys) as ETL, followed by a 35 nm layer of SnO_x (Tetrakis(dimethylamino)tin(IV)) (TDMAStn, Strem Chemicals, 1066-77-9) via atomic layer deposition. As recombination layer, a 15 nm thick ITO thin film was deposited via d.c. sputtering. Subsequently, the aqueous PEDOT:PSS solution was diluted in ethanol with a 3:1 ratio and deposited via spin coating at 6000 r.p.m. for 30 s and a annealing step at 120 °C for 20 min. The narrow band gap perovskite was prepared by adding a 1 M perovskite solution with 275 mg FAI, 63.6 mg MAI, 372 mg SnI₂, 469 mg PbI₂, 10.43 mg Pb(SCN)₂ and 3.73 mg SnF₂ within a 9:1 DMF:DMSO mixture to 32 µl of a 1.5 M CsI solution in DMSO. The solution was deposited via spin coating at 6000 r.p.m. for 12 s and the substrate immediately afterwards transferred in a vacuum chamber with 10 Pa and 150 ml volume, followed by an annealing step at 100 °C for 7 min. Subsequently, a 5 nm thick PCBM layer was deposited from a 1,2-dichlorobenzene (Sigma-Aldrich) solution, followed by 25 nm of C_{60} , 7 nm of bathocuproine (BCP, Luminescence Technology, CAS: 4733-39-5) and 75 nm of gold via thermal evaporation. Finally, a 125 nm thick magnesium fluoride (MgF₂, Sigma-Aldrich, CAS: 7783-40-6) thin film was thermally evaporated on the front side of the glass as anti-reflection coating. The deposition of both absorber layers was optimized in order to achieve a layer thickness of 400 nm for the WBG perovskite and of 800 nm for the NBG perovskite. For fabrication of two-terminal perovskite-perovskite tandem solar modules only scalable fabrication methods were used. Therefore, spin coating deposition steps were replaced with a combination of vacuum deposition and blade coating. To avoid lateral shunting between the back electrode and the recombination layer via P2 scribing line of modules, the ITO recombination layer was replaced with a thermally evaporated 1.2 nm thick percolated gold layer.

Laser scribing:

The scribing of individual scribing lines for fabrication of module interconnections (P1, P2, P3) and transparent areas in devices (P4) was performed with a custom-built laser scribing setup (Bergfeld Lasertech GmbH). The setup comprises a 1 ns Nd:YVO₄ laser (Picolo AOT 10-MOPA, InnoLas Laser GmbH) with wavelengths of 1064 and 532 nm at variably power output, a scanner system, a camera for alignment and an air ventilation and filtering circuit. To ensure accurate dimensions of scribing layouts, the system was calibrated via optical microscope (Leitz Wetzlar). Prevention of degradation of devices due to contact with ambient atmosphere was enabled by incorporating the system in a nitrogen-filled glovebox. The P1 scribing process employed a scribing speed of 50 mm s⁻¹ and a laser pulse fluence of 2 J cm⁻². Following the deposition of the functional layers (ETL, absorber, HTL), the P2 scribing process was carried out at a scribing speed of 33 mm s⁻¹ and a laser pulse fluence of 0.35 J cm⁻². After deposition of the back electrode, the P3 scribing process was performed at a scribing speed of 100 mm s⁻¹ and a laser pulse fluence of 0.3 J cm⁻². The P4 scribing process for fabrication of transparent areas in all single-junction solar cells and submodules employed a scribing speed of 100 mm s⁻¹ and a laser pulse fluence of 0.17 J cm⁻². For the optional second P4 scribing process, a scribing speed of 100 mm/s and a laser pulse fluence of 1.3 J cm⁻² was employed. All scribing processes were carried out from the film side at a laser pulse frequency of 10 kHz and a laser wavelength of 532 nm.

Characterization:

Microscopy images were taken with a BH2-UMA microscope (Olympus Corporation). For measurement of transmittance, diffuse transmittance, reflectance, haze and EQE spectra of fabricated devices a Bentham PVE300 photovoltaic device characterization system was employed. Resulting from the device's integrating sphere and port dimensions, diffuse transmittance and haze were measured for a deviation of greater 3.8° from the direction of incidence. Monochromatic light was modulated with a chopper frequency of 600 Hz. The AVT, the CIELAB chromaticity coordinates (L^* , a^* , b^*) and the color rendering indices (CRI) for translucent device areas were calculated from measured transmittance spectra via in-house MATLAB script, following the definition and calculation approach reported elsewhere.^{3,4} Current-density-voltage (J-V) characteristics were performed with a solar simulator (Newport Oriel Sol3A) under global standard radiation (AM1.5G). Light intensity was calibrated via silicon reference solar cell integrating a KG5 short pass filter. J-V scans were carried out in forward and backward direction with scanning speeds of about 0.6 V s⁻¹. Continuous tracking of the maximum power point (MPP) was conducted by utilizing a perturb-and-observe algorithm. During measurements, solar cells and modules were not actively cooled.

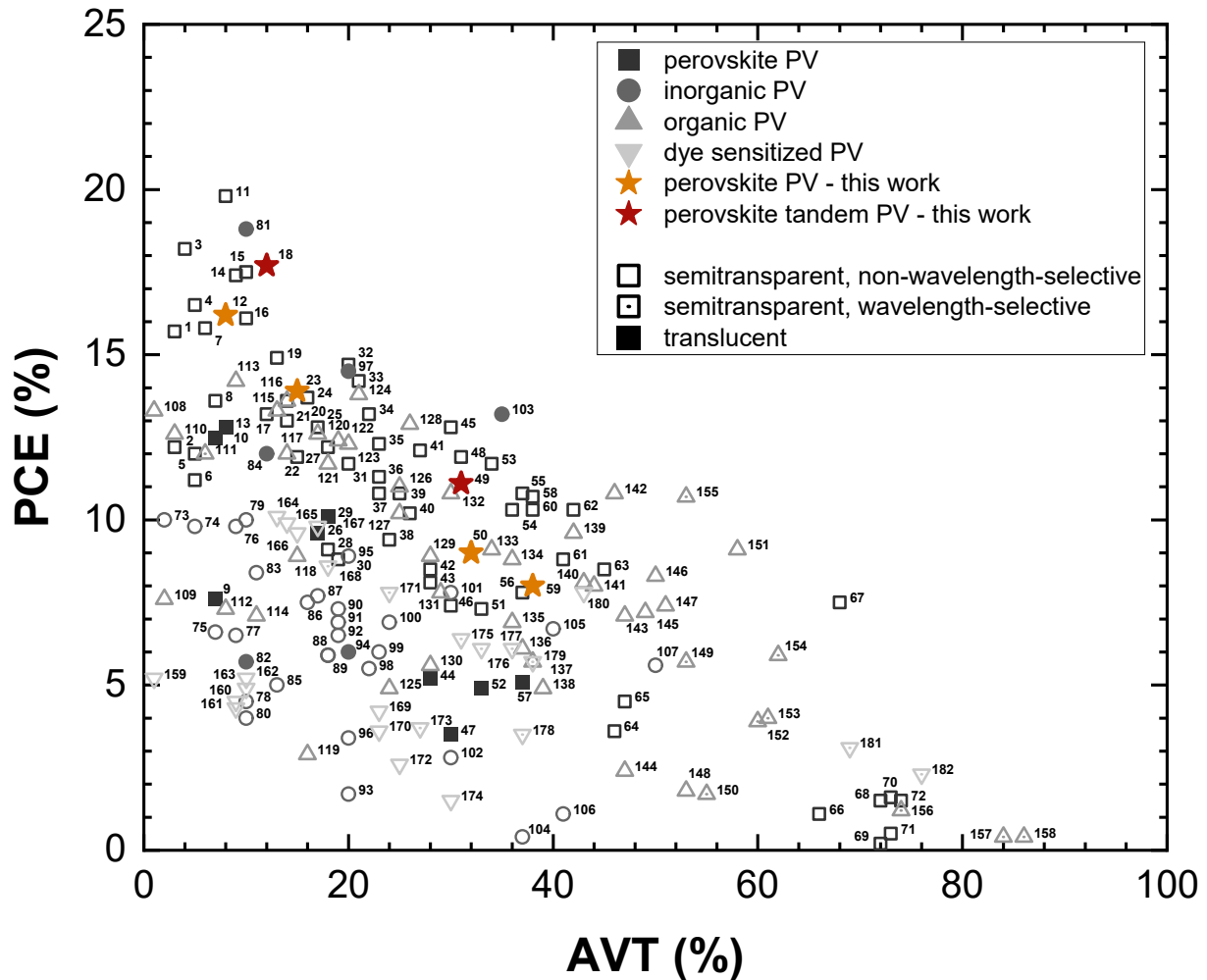


Figure S1. Power conversion efficiencies as a function of average visible transmittance for transparent photovoltaics being based on different technological approaches. Detailed information about the data points is summarized in Table S1 in the Supplemental Information.

Table S1. Comparison of photovoltaic parameters of transparent solar cells and modules reported in literature. Data is sorted by absorber type and average visible transmittance.

label number	authors	source	absorber type	transparent PV technology	device	AVT (%)	PCE (%)	V _{oc} (mV)	J _{sc} (mA cm ⁻²)	FF (%)	LUE (%)	absorber	bandgap (eV)
1	Lim, S.-H. <i>et al.</i>	5	perovskite PV	st, nws	cell	3	15.7	1070	19.0	77.2	0.47	Cs _{0.175} FA _{0.75} MA _{0.075} Pb(I _{0.875} Br _{0.125}) ₃	1.64
2	Li, C. <i>et al.</i>	6	perovskite PV	st, nws	cell	3	12.2	1017	17.5	68.5	0.37	MAPbI ₃	1.53
3	Ying, Z. <i>et al.</i>	7	perovskite PV	st, nws	cell	4	18.2	1076	21.1	80.0	0.73	CsFAMAPb(IV) ₃	1.63
4	Chen, B. <i>et al.</i>	8	perovskite PV	st, nws	cell	5	16.5	1080	20.6	74.2	0.83	MAPbI ₃	1.60
5	You, P. <i>et al.</i>	9	perovskite PV	st, nws	cell	5	12.0	960	19.2	65.3	0.60	MAPbI _{3-x} Cl _x	1.61
6	Jang, C. W. <i>et al.</i>	10	perovskite PV	st, nws	cell	5	11.2	940	18.4	64.9	0.56	MAPbI ₃	1.65
7	Heo, J. H. <i>et al.</i>	11	perovskite PV	st, nws	cell	6	15.8	1100	19.3	74.4	0.95	MAPbI ₃	1.60
8	Gaspera, E. D. <i>et al.</i>	12	perovskite PV	st, nws	cell	7	13.6	988	20.4	67.5	0.95	MAPbI ₃	1.55
9	Eperon, G. E. <i>et al.</i>	13	perovskite PV	translucent	cell	7	7.6	760	15.2	61.0	0.53	CH ₃ NH ₃ PbI _(3-x) Cl _x	1.48
10	Rakocevic, L. <i>et al.</i>	14	perovskite PV	translucent	cell	7	12.5	950	18.6	72.0	0.91	CH ₃ NH ₃ PbI _(3-x) Cl _x	n/a
11	Yang, D. <i>et al.</i>	15	perovskite PV	st, nws	cell	8	19.8	1137	21.9	79.5	1.58	Cs _{0.05} FA _{0.95} PbI ₃	1.52
12	this work	-	perovskite PV	translucent	cell	8	16.2	1081	19.0	79.0	1.30	Cs _{0.05} MA _{0.1} FA _{0.85} Pb(I _{0.9} Br _{0.1}) ₃	1.59
13	Rakocevic, L. <i>et al.</i>	14	perovskite PV	translucent	cell	8	12.8	963	18.4	74.0	0.97	CH ₃ NH ₃ PbI _(3-x) Cl _x	n/a
14	Lim, S.-H. <i>et al.</i>	5	perovskite PV	st, nws	cell	9	17.4	1083	21.5	75.1	1.57	Cs _{0.175} FA _{0.825} Pb(I _{0.875} Br _{0.125}) ₃	1.64
15	Yuan, L. <i>et al.</i>	16	perovskite PV	st, nws	cell	10	17.5	1070	22.4	73.1	1.75	MAPbI ₃	1.59
16	Yu, J. C. <i>et al.</i>	17	perovskite PV	st, nws	cell	10	16.1	1060	20.4	74.5	1.61	Cs _{0.05} (FA _{0.85} MA _{0.15}) _{0.95} Pb(I _{0.85} Br _{0.15}) ₃	1.65
17	Yuan, L. <i>et al.</i>	16	perovskite PV	st, nws	cell	12	13.2	1000	19.5	67.8	1.58	MAPbI ₃	1.60
18	this work	-	perovskite tandem PV	translucent	cell	12	17.7	1950	11.9	77.0	2.12	Cs _x (FA _{0.83} MA _{0.17}) _(1-x) Sn _{0.5} Pb _{0.5} I ₃ , FA _{0.8} Cs _{0.2} (I _{0.6} Br _{0.4}) ₃	1.26, 1.78

19	Yuan, L. <i>et al.</i>	¹⁶	perovskite PV	st, nws	cell	13	14.9	1100	19.8	68.4	1.94	MAPbI _{2.5} Br _{0.5}	1.67
20	Lim, S.-H. <i>et al.</i>	⁵	perovskite PV	st, nws	cell	14	13.6	1048	16.5	78.6	1.90	Cs _{0.175} FA _{0.825} Pb(I _{0.875} Br _{0.125}) ₃	1.64
21	Ramírez Quiroz, C. O. <i>et al.</i>	¹⁸	perovskite PV	st, nws	cell	14	13.0	970	19.1	69.9	1.82	MAPbI _{3-x} Cl _x	1.57
22	Yuan, L. <i>et al.</i>	¹⁶	perovskite PV	st, nws	cell	15	11.9	1000	17.8	66.3	1.79	MAPbI ₃	1.61
23	this work	-	perovskite PV	translucent	cell	15	13.9	1085	16.2	79.0	2.09	Cs _{0.05} MA _{0.1} FA _{0.85} Pb(I _{0.9} Br _{0.1}) ₃	1.59
24	Yuan, L. <i>et al.</i>	¹⁶	perovskite PV	st, nws	cell	16	13.7	1120	16.7	73.4	2.19	MAPbI ₂ Br	1.76
25	Yu, J. C. <i>et al.</i>	¹⁷	perovskite PV	st, nws	cell	17	12.8	1040	16.6	74.1	2.18	Cs _{0.05} (FA _{0.85} MA _{0.15}) _{0.95} Pb(I _{0.85} Br _{0.15}) ₃	1.65
26	Rakocevic, L. <i>et al.</i>	¹⁴	perovskite PV	translucent	cell	17	9.6	938	14.9	70.0	1.65	CH ₃ NH ₃ PbI _(3-x) Cl _x	n/a
27	Yuan, L. <i>et al.</i>	¹⁶	perovskite PV	st, nws	cell	18	12.2	1110	15.1	72.7	2.20	MAPbI ₂ Br	1.77
28	Li, C. <i>et al.</i>	⁶	perovskite PV	st, nws	cell	18	9.1	1017	14.6	61.5	1.64	MAPbI ₃	1.53
29	Rakocevic, L. <i>et al.</i>	¹⁴	perovskite PV	translucent	cell	18	10.1	950	14.8	73.0	1.82	CH ₃ NH ₃ PbI _(3-x) Cl _x	n/a
30	Gaspera, E. D. <i>et al.</i>	¹²	perovskite PV	st, nws	cell	19	8.8	941	13.7	68.3	1.67	MAPbI ₃	1.55
31	Zhang, Y.-W. <i>et al.</i>	¹⁹	perovskite PV	st, nws	cell	20	11.7	1080	14.5	74.6	2.34	MAPbI ₃ + BiPy - I	1.63
32	Dou, Y. <i>et al.</i>	²⁰	perovskite PV	st, nws	cell	20	14.7	1108	17.6	75.2	2.94	K _x Cs _{0.05} (FA _{0.85} MA _{0.15}) _{0.95} Pb(I _{0.85} Br _{0.15}) ₃	1.63
33	Dou, Y. <i>et al.</i>	²⁰	perovskite PV	st, nws	cell	21	14.2	1117	17.4	73.2	2.98	K _x Cs _{0.05} (FA _{0.85} MA _{0.15}) _{0.95} Pb(I _{0.85} Br _{0.15}) ₃	1.63
34	Dou, Y. <i>et al.</i>	²⁰	perovskite PV	st, nws	cell	22	13.2	1073	17.2	71.7	2.90	K _x Cs _{0.05} (FA _{0.85} MA _{0.15}) _{0.95} Pb(I _{0.85} Br _{0.15}) ₃	1.61
35	Dou, Y. <i>et al.</i>	²⁰	perovskite PV	st, nws	cell	23	12.3	1082	17.1	66.6	2.83	K _x Cs _{0.05} (FA _{0.85} MA _{0.15}) _{0.95} Pb(I _{0.85} Br _{0.15}) ₃	1.61
36	Xiao, S. <i>et al.</i>	²¹	perovskite PV	st, nws	cell	23	11.3	1040	15.1	72.3	2.60	MAPbI ₃	1.62
37	Ramírez Quiroz, C. O. <i>et al.</i>	¹⁸	perovskite PV	st, nws	cell	23	10.8	970	17.3	64.4	2.48	MAPbI _{3-x} Cl _x	1.57
38	Yuan, L. <i>et al.</i>	¹⁶	perovskite PV	st, nws	cell	24	9.4	1120	13.6	61.6	2.26	MAPbI _{1.5} Br _{1.5}	1.87
39	Chang, C.-Y. <i>et al.</i>	²²	perovskite PV	st, nws	cell	25	10.8	950	16.3	69.7	2.70	MAPbI ₃	1.55

40	Jung, J. W. <i>et al.</i>	²³	perovskite PV	st, nws	cell	26	10.2	1070	12.2	78.1	2.65	MAPbI ₃	1.63
41	Yuan, L. <i>et al.</i>	¹⁶	perovskite PV	st, nws	cell	27	12.1	1000	18.3	66.2	3.27	MAPbI ₃	1.60
42	Guo, F. <i>et al.</i>	²⁴	perovskite PV	st, nws	cell	28	8.5	964	13.1	66.8	2.38	MAPbI _{3-x} Cl _x	1.6
43	Ramírez Quiroz, C. O. <i>et al.</i>	¹⁸	perovskite PV	st, nws	cell	28	8.1	1030	11.2	70.2	2.27	MAPbI _{3-x} Cl _x	1.57
44	Eperon, G. E. <i>et al.</i>	²⁵	perovskite PV	translucent	cell	28	5.2	740	11.8	58.0	1.46	CH ₃ NH ₃ PbI _(3-x) Cl _x	1.48
45	Kwon, H.-C. <i>et al.</i>	²⁶	perovskite PV	st, nws	cell	30	12.8	1030	16.5	74.9	3.84	MAPbI _{3-x} Cl _x	1.62
46	Yu, J. C. <i>et al.</i>	¹⁷	perovskite PV	st, nws	cell	30	7.4	1010	11.8	62.2	2.22	Cs _{0.05} (FA _{0.85} MA _{0.15}) _{0.95} Pb(I _{0.85} Br _{0.15}) ₃	1.65
47	Eperon, G. E. <i>et al.</i>	¹³	perovskite PV	translucent	cell	30	3.5	710	8.1	61.0	1.05	CH ₃ NH ₃ PbI _(3-x) Cl _x	1.48
48	Yuan, L. <i>et al.</i>	¹⁶	perovskite PV	st, nws	cell	31	11.9	1050	16.3	69.4	3.69	MAPbI _{2.5} Br _{0.5}	1.69
49	this work	-	perovskite tandem PV	translucent	cell	31	11.1	1940	8.1	71.0	3.44	Cs _x (FA _{0.83} MA _{0.17}) _(1-x) Sn _{0.5} Pb _{0.5} I ₃ , FA _{0.8} Cs _{0.2} (I _{0.6} Br _{0.4}) ₃	1.26, 1.78
50	this work	-	perovskite PV	translucent	module	32	9.0	5500	11.1	74.0	2.88	Cs _{0.17} FA _{0.83} Pb(I _{0.92} Br _{0.08}) ₃	1.61
51	Roldán-Carmona, C. <i>et al.</i>	²⁷	perovskite PV	st, nws	cell	33	7.3	1037	13.4	52.5	2.41	MAPbI ₃	1.55
52	Rakocevic, L. <i>et al.</i>	¹⁴	perovskite PV	translucent	cell	33	4.9	950	9.3	60.0	1.62	CH ₃ NH ₃ PbI _(3-x) Cl _x	n/a
53	Kwon, H.-C. <i>et al.</i>	²⁶	perovskite PV	st, nws	cell	34	11.7	990	15.9	74.6	3.98	MAPbI _{3-x} Cl _x	1.62
54	Yuan, L. <i>et al.</i>	¹⁶	perovskite PV	st, nws	cell	36	10.3	1080	14.6	65.5	3.71	MAPbI ₂ Br	1.79
55	Kwon, H.-C. <i>et al.</i>	²⁶	perovskite PV	st, nws	cell	37	10.8	1010	14.7	73.1	4.00	MAPbI _{3-x} Cl _x	1.62
56	Ramírez Quiroz, C. O. <i>et al.</i>	¹⁸	perovskite PV	st, nws	cell	37	7.8	970	11.6	69.6	2.89	MAPbI _{3-x} Cl _x	1.57
57	Rakocevic, L. <i>et al.</i>	¹⁴	perovskite PV	translucent	cell	37	5.1	938	8.6	72.0	1.89	CH ₃ NH ₃ PbI _(3-x) Cl _x	n/a
58	Jung, J. W. <i>et al.</i>	²³	perovskite PV	st, nws	cell	38	10.7	1060	13	77.6	4.07	MAPbI ₃	1.63
59	this work	-	perovskite PV	translucent	cell	38	8.0.	1080	9.6	77.0	3.04	Cs _{0.05} MA _{0.1} FA _{0.85} Pb(I _{0.9} Br _{0.1}) ₃	1.59
60	Zhang, L. <i>et al.</i>	²⁸	perovskite PV	st, nws	cell	38	10.3	980	15.7	66.0	3.91	MAPb(I _(3-x) Br _(x)) ₃	n/a

61	Yuan, L. <i>et al.</i>	¹⁶	perovskite PV	st, nws	cell	41	8.8	1110	12.8	62.2	3.61	MAPbI _{1.5} Br _{1.5}	1.90
62	Kwon, H.-C. <i>et al.</i>	²⁶	perovskite PV	st, nws	cell	42	10.3	1000	13.6	75.6	4.33	MAPbI _{3-x} Cl _x	1.63
63	Kwon, H.-C. <i>et al.</i>	²⁶	perovskite PV	st, nws	cell	45	8.5	960	12.6	73.5	3.83	MAPbI _{3-x} Cl _x	1.64
64	Ramírez Quiroz, C. O. <i>et al.</i>	¹⁸	perovskite PV	st, nws	cell	46	3.6	1030	5.4	64.4	1.66	MAPbI _{3-x} Cl _x	1.57
65	Bag, S. <i>et al.</i>	²⁹	perovskite PV	st, nws	cell	47	4.5	880	8.2	63.0	2.12	MAPbI ₃	1.63
66	Liu, G. <i>et al.</i>	³⁰	perovskite PV	st, nws	cell	66	1.1	1000	2.1	52.9	0.73	Cs ₂ AgBiBr ₆	2.62
67	Zuo, L. <i>et al.</i>	³¹	perovskite PV	st, nws	cell	68	7.5	1550	6.7	72.0	5.10	FAPbBr _{2.43} Cl _{0.57}	2.35
68	Liu, G. <i>et al.</i>	³⁰	perovskite PV	st, nws	cell	72	1.5	960	2.1	74.3	1.08	Cs ₂ AgBiBr ₆	2.62
69	Liu, D. <i>et al.</i>	³²	perovskite PV	st, nws	cell	72	0.2	1110	0.6	35.4	0.14	MAPbCl ₃	3.03
70	Liu, G. <i>et al.</i>	³⁰	perovskite PV	st, nws	cell	73	1.6	970	2.2	73.1	1.17	Cs ₂ AgBiBr ₆	2.62
71	Liu, D. <i>et al.</i>	³²	perovskite PV	st, nws	cell	73	0.5	1260	0.9	44.9	0.37	MAPbCl _{2.4} Br _{0.6}	2.84
72	Liu, G. <i>et al.</i>	³⁰	perovskite PV	st, nws	cell	74	1.5	970	2.2	71.1	1.11	Cs ₂ AgBiBr ₆	2.62
73	Shin, M. J. <i>et al.</i>	³³	inorganic PV	st, nws	cell	2	10	640	23.3	66.9	0.20	CIGS	1.23
74	Shin, M. J. <i>et al.</i>	³⁴	inorganic PV	st, nws	cell	5	9.8	630	22.9	67.6	0.49	CIGS	1.26
75	Kim, J. <i>et al.</i>	³⁵	inorganic PV	st, nws	cell	7	6.6	881	11.8	63.7	0.46	a-Si:H	1.92
76	Shin, M. J. <i>et al.</i>	³³	inorganic PV	st, nws	cell	9	9.8	630	20.9	74.1	0.88	CIGS	1.30
77	Kim, K. <i>et al.</i>	³⁶	inorganic PV	st, nws	cell	9	6.5	597	22.9	46.5	0.59	CIGS	1.28
78	ASI THRU thin-film solar module, semitransparent, SCHOTT Solar GmbH	³⁷	inorganic PV	st, nws	module	10	4.5	49000	0.17	n/a	0.45	a-Si/μ-Si	n/a
79	PS-CT series panels, Polysolar Limited	³⁸	inorganic PV	st, nws	module	10	10	87000	0.11	n/a	1.00	CdTe	1.54
80	Amorphous Silicon PV Glass, Onyx Solar Group LLC	³⁹	inorganic PV	st, nws	module	10	4.0	n/a	n/a	n/a	0.40	a-Si:H	n/a
81	PS-MC-ST series panels, Polysolar Limited	⁴⁰	inorganic PV	translucent	module	10	18.8	39700	0.6	n/a	1.88	mono c-Si	n/a

82	VOLTARLUX ASI-Glas, Glaswerke Arnold GmbH & Co. KG	⁴¹	inorganic PV	translucent	module	10	5.7	111000	0.08	n/a	0.57	a-Si/ μ -Si	n/a
83	Shin, M. J. <i>et al.</i>	³⁴	inorganic PV	st, nws	cell	11	8.4	620	20.4	66.3	0.92	CIGS	1.34
84	Kuk, S. <i>et al.</i>	⁴²	inorganic PV	translucent	cell	12	12	670	20.6	69.0	1.44	CIGS	n/a
85	Yang, R. <i>et al.</i>	⁴³	inorganic PV	st, nws	cell	13	5.0	864	9.9	58.1	0.65	a-Si:H	1.75
86	Cho, J.-S. <i>et al.</i>	⁴⁴	inorganic PV	st, nws	cell	16	7.5	810	14.2	65.3	1.20	a-Si:H	1.83
87	Cho, J.-S. <i>et al.</i>	⁴⁴	inorganic PV	st, nws	cell	17	7.7	810	14.1	67.3	1.31	a-Si:H	1.83
88	Lim, J. W. <i>et al.</i>	⁴⁵	inorganic PV	st, nws	cell	18	5.9	720	14.1	58.3	1.06	a-SiGe:H	2.05
89	Saifullah, M. <i>et al.</i>	⁴⁶	inorganic PV	st, nws	cell	18	5.9	710	14.6	57.4	1.06	CIGS	1.50
90	Cho, J.-S. <i>et al.</i>	⁴⁴	inorganic PV	st, nws	cell	19	7.3	820	13.1	67.6	1.39	a-Si:H	1.87
91	Shin, M. J. <i>et al.</i>	³⁴	inorganic PV	st, nws	cell	19	6.9	640	16.6	64.7	1.31	CIGS	1.30
92	Shin, M. J. <i>et al.</i>	³³	inorganic PV	st, nws	cell	19	6.5	580	17.5	63.5	1.24	CIGS	1.34
93	Moon, S. H. <i>et al.</i>	⁴⁷	inorganic PV	st, nws	cell	20	1.7	495	8.9	40.8	0.34	CIGS	1.64
94	Tsai, C. Y. <i>et al.</i>	⁴⁸	inorganic PV	translucent	cell	20	6.0	418	24.2	60.0	1.20	a-Si/ μ -Si	n/a
95	PS-CT series panels, Polysolar Limited	³⁸	inorganic PV	st, nws	module	20	8.9	87000	0.1	n/a	1.78	CdTe	1.54
96	Amorphous Silicon PV Glass, Onyx Solar Group LLC	³⁹	inorganic PV	st, nws	module	20	3.4	n/a	n/a	n/a	0.68	a-Si:H	n/a
97	Park, J. <i>et al.</i>	⁴⁹	inorganic PV	translucent	cell	20	14.5	638	28.9	79.0	2.90	c-Si	1.10
98	Lim, J. W. <i>et al.</i>	⁴⁵	inorganic PV	st, nws	cell	22	5.5	760	12.3	58.6	1.21	a-Si:H	2.05
99	Cho, J.-S. <i>et al.</i>	⁴⁴	inorganic PV	st, nws	cell	23	6.0	830	10.6	68.2	1.38	a-Si:H	1.92
100	Lim, J. W. <i>et al.</i>	⁵⁰	inorganic PV	st, nws	cell	24	6.9	920	10.7	70.3	1.66	a-Si:H	1.68
101	PS-CT series panels, Polysolar Limited	³⁸	inorganic PV	st, nws	module	30	7.8	87000	0.08	n/a	2.34	CdTe	1.54

102	Amorphous Silicon PV Glass, Onyx Solar Group LLC	39	inorganic PV	st, nws	module	30	2.8	n/a	n/a	n/a	0.84	a-Si:H	n/a
103	Aleo Solar PV Isolierglas Isolante, Aleo Solar GmbH	51	inorganic PV	translucent	module	35	13.2	26800	0.6	n/a	4.62	mono c-Si	n/a
104	Mutalikdesai, A. et al.	52	inorganic PV	st, nws	cell	37	0.4	101	14.7	27.2	0.15	CdTe	1.54
105	PS-CT series panels, Polysolar Limited	38	inorganic PV	st, nws	module	40	6.7	87000	0.08	n/a	2.68	CdTe	1.54
106	Kim, S. et al.	53	inorganic PV	st, nws	cell	41	1.1	596	3.9	47.3	0.45	a-Si:H	2.17
107	PS-CT series panels, Polysolar Limited	38	inorganic PV	st, nws	module	50	5.6	87000	0.06	n/a	2.80	CdTe	1.54
108	Sung, Y.-M. et al.	54	organic PV	st, nws	cell	1	13.3	810	24.6	66.5	0.13	PM6:Y6	1.40
109	Chen, K.-S. et al.	55	organic PV	st, nws	cell	2	7.6	770	15.6	63.3	0.15	PBDTTT-C-T:PC ₇₁ BM	1.66
110	Sung, Y.-M. et al.	54	organic PV	st, nws	cell	3	12.6	800	24.5	64.5	0.38	PM6:Y6	1.40
111	Wang, C.-K. et al.	56	organic PV	st, ws	cell	6	12	870	19.6	70.4	0.72	PM7/PTTtID-Cl/IT-4F	1.47
112	Sung, Y.-M. et al.	54	organic PV	st, nws	cell	8	7.3	860	12.1	69.6	0.58	DTDCPB:C ₇₀	1.73
113	Hu, Z. et al.	57	organic PV	st, nws	cell	9	14.2	854	23.0	72.3	1.28	PM6:Y6	1.42
114	Chen, K.-S. et al.	55	organic PV	st, nws	cell	11	7.1	760	14.5	64.4	0.78	PBDTTT-C-T:PC ₇₁ BM	1.66
115	Hu, Z. et al.	57	organic PV	st, nws	cell	13	13.3	853	21.7	71.9	1.73	PM6:Y6	1.42
116	Li, X. et al.	58	organic PV	st, nws	cell	14	13.6	850	21.1	75.8	1.90	PM6:Y6	1.40
117	Song, W. et al.	59	organic PV	st, nws	cell	14	12.0	844	19.6	72.8	1.68	PM6:Y6:C6	1.41
118	Xiao, T. et al.	60	organic PV	st, nws	cell	15	8.9	772	18.3	63.0	1.34	PTB7-Th:FNIC1	1.52
119	Wageh, S. et al.	61	organic PV	st, nws	cell	16	2.9	540	9.7	55.4	0.46	P3HT-PCBM	1.95
120	Song, W. et al.	62	organic PV	st, nws	cell	17	12.6	810	21.2	73.2	2.14	PBDB-T-2F:Y6	1.39
121	Song, W. et al.	62	organic PV	st, nws	cell	18	11.7	810	20.7	69.6	2.11	PBDB-T-2F:Y6	1.39
122	Hu, Z. et al.	57	organic PV	st, nws	cell	19	12.4	852	20.4	71.4	2.36	PM6:Y6	1.42

123	Bai, Y. <i>et al.</i>	⁶³	organic PV	st, nws	cell	20	12.3	817	20.6	73.0	2.46	PM6:Y6	1.42
124	Chang, L. <i>et al.</i>	⁶⁴	organic PV	st, nws	cell	21	13.8	820	25.3	66.5	2.90	PM6:N3	1.41
125	Riede, M. <i>et al.</i>	⁶⁵	organic PV	st, nws	cell	24	4.9	1.58	5.2	61.0	1.17	F4-ZnPc:C60, DCV6T:C60	n/a
126	Yi, L. <i>et al.</i>	⁶³	organic PV	st, nws	cell	25	11.0	750	20.9	70.0	2.75	PCE-10:A078	1.34
127	Yao, M. <i>et al.</i>	⁶⁵	organic PV	st, nws	cell	25	10.2	736	20.3	68.3	2.55	PTB7-Th:FOIC	1.40
128	Bai, Y. <i>et al.</i>	⁶⁶	organic PV	st, nws	cell	26	12.9	825	21.6	72.4	3.35	PBDB-T-2F:Y6	1.40
129	Chang, L. <i>et al.</i>	⁶⁴	organic PV	st, nws	cell	28	8.9	810	16.8	65.1	2.49	PM6:N3	1.41
130	Chen, K.-S. <i>et al.</i>	⁵⁵	organic PV	st, nws	cell	28	5.6	760	11.9	61.9	1.57	PBDTTT-C-T:PC ₇₁ BM	1.66
131	Chang, L. <i>et al.</i>	⁶⁴	organic PV	st, nws	cell	29	7.8	800	15.2	64.7	2.26	PM6:N3	1.41
132	Xia, R. <i>et al.</i>	⁶⁷	organic PV	st, nws	cell	30	10.8	718	21.9	68.7	3.24	PTB7-Th:IEICO-4F	1.35
133	Yao, M. <i>et al.</i>	⁶⁵	organic PV	st, nws	cell	34	9.1	733	18.5	67.1	3.09	PTB7-Th:FOIC	1.40
134	Li, Y. <i>et al.</i>	⁶⁸	organic PV	st, nws	cell	36	8.8	680	18	71.9	3.17	PCE-10:BT-CIC:TT-FIC	1.37
135	Jose da Silva, W. <i>et al.</i>	⁶⁹	organic PV	st, nws	cell	36	6.9	890	11.6	66.5	2.48	PSEHTT:ICBA	1.86
136	Jose da Silva, W. <i>et al.</i>	⁶⁹	organic PV	st, nws	cell	37	6.1	890	10.2	66.8	2.26	PSEHTT:ICBA	1.86
137	Song, S. <i>et al.</i>	⁷⁰	organic PV	st, nws	cell	38	5.7	700	12.4	66.2	2.17	PTB7-Th:IEICO-4F	1.33
138	Jose da Silva, W. <i>et al.</i>	⁶⁹	organic PV	st, nws	cell	39	4.9	880	8.3	67.9	1.91	PSEHTT:ICBA	1.86
139	Corzo, D. <i>et al.</i>	⁷¹	organic PV	st, nws	cell	42	9.6	690	26.1	53.2	4.03	PTB7-Th:IEICO-4F	1.35
140	Li, Y. <i>et al.</i>	⁶³	organic PV	st, nws	cell	43	8.1	730	16.3	68.1	3.48	PCE-10:A078	1.34
141	Li, Y. <i>et al.</i>	⁶⁸	organic PV	st, nws	cell	44	8.0	680	16.2	72.6	3.52	PCE-10:BT-CIC:TT-FIC	1.37
142	Li, Y. <i>et al.</i>	⁶³	organic PV	st, nws	cell	46	10.8	750	20.4	70.6	4.97	PCE-10:A078	1.34
143	Li, Y. <i>et al.</i>	⁶³	organic PV	st, nws	cell	47	7.1	730	14.3	68.0	3.34	PCE-10:A078	1.34
144	Jose da Silva, W. <i>et al.</i>	⁶⁹	organic PV	st, nws	cell	47	2.4	860	4.1	68.2	1.13	PSEHTT:ICBA	1.86

145	Li, Y. <i>et al.</i>	⁶⁸	organic PV	st, nws	cell	49	7.2	670	14.8	72.6	3.53	PCE-10:BT-CIC:TT-FIC	1.37
146	Liu, Q. <i>et al.</i>	⁷²	organic PV	st, nws	cell	50	8.3	746	16.7	66.8	4.15	PTB7-Th:FOIC:PC71BM	1.38
147	Liu, Q. <i>et al.</i>	⁷²	organic PV	st, nws	cell	51	7.4	749	14.7	66.7	3.77	PTB7-Th:FOIC:PC71BM	1.39
148	Jose da Silva, W. <i>et al.</i>	⁶⁹	organic PV	st, nws	cell	53	1.8	890	3.8	54.8	0.95	PSEHTT:ICBA	1.86
149	Lee, J. <i>et al.</i>	⁷³	organic PV	st, ws	cell	53	5.7	750	10.6	69.5	3.02	DPP2T:IEICO-4F	1.32
150	Lunt, R. R. <i>et al.</i>	⁷⁴	organic PV	st, ws	cell	55	1.7	450	4.0	70.0	0.94	C1A1Pc	1.47
151	Chaturverdi, N. <i>et al.</i>	⁷⁵	organic PV	st, nws	cell	58	9.1	680	22.6	59.1	5.28	PTB7-Th:IEICO-4F	1.32
152	Lee, J. <i>et al.</i>	⁷³	organic PV	st, ws	cell	60	3.9	749	7.3	70.2	2.34	DPP2T:IEICO-4F	1.33
153	Chen, C. C. <i>et al.</i>	⁷⁶	organic PV	st, ws	cell	61	4.0	770	9.3	56.0	2.44	PBDTT-DPP:PCBM	1.55
154	Zuo, L. <i>et al.</i>	³¹	organic PV	st, ws	cell	62	5.9	690	12.9	66.0	3.66	PTB7-Th:6TIC-4F	1.33
155	Zuo, L. <i>et al.</i>	³¹	organic PV	st, ws	cell	53	10.7	2200	6.1	74.0	5.67	PTB7-Th:6TIC-4F, FAPbBr _{2.43} Cl _{0.57}	3.56
156	Yang, C. <i>et al.</i>	⁷⁷	organic PV	st, ws	cell	74	1.2	990	1.5	81.0	0.89	CO ₈ DFIC	1.50
157	Zhao, Y. <i>et al.</i>	⁷⁸	organic PV	st, ws	cell	84	0.4	520	1.3	65.0	0.34	PBMMA:PEMA: (TBA) ₂ Mo ₆ Cl ₁₄	2.81
158	Zhao, Y. <i>et al.</i>	⁷⁹	organic PV	st, ws	cell	86	0.4	500	1.2	66.0	0.34	Cy7	1.52
159	López-López, C. <i>et al.</i>	⁸⁰	dye sensitized PV	st, nws	cell	1	5.2	780	12.4	53.7	0.05	N719	2.00
160	López-López, C. <i>et al.</i>	⁸⁰	dye sensitized PV	st, nws	cell	9	4.5	780	10.3	56.0	0.41	N719	2.00
161	Colonna, D. <i>et al.</i>	⁸¹	dye sensitized PV	st, nws	cell	9	4.3	720	9.9	60.0	0.39	N719+SDA	1.82
162	Colonna, D. <i>et al.</i>	⁸¹	dye sensitized PV	st, nws	cell	10	5.2	770	11.9	57.0	0.52	N719	2.01
163	López-López, C. <i>et al.</i>	⁸⁰	dye sensitized PV	st, nws	cell	10	4.9	765	11.4	56.1	0.49	N719	2.00
164	Aftabuzzaman, M. <i>et al.</i>	⁸²	dye sensitized PV	st, nws	cell	13	10.1	851	14.9	80.2	1.31	SGT-021	1.68
165	Aftabuzzaman, M. <i>et al.</i>	⁸²	dye sensitized PV	st, nws	cell	14	9.9	850	14.9	78.5	1.37	SGT-021	1.68

166	Aftabuzzaman, M. <i>et al.</i>	⁸²	dye sensitized PV	st, nws	cell	15	9.6	850	14.7	77.2	1.44	SGT-021	1.68
167	Aftabuzzaman, M. <i>et al.</i>	⁸²	dye sensitized PV	st, nws	cell	17	9.8	855	15.1	75.5	1.67	SGT-021	1.68
168	Chalkias, D. A. <i>et al.</i>	⁸³	dye sensitized PV	st, ws	cell	18	8.6	750	16.7	68.4	1.55	N719 (EtOH)	2.00
169	Colonna, D. <i>et al.</i>	⁸¹	dye sensitized PV	st, nws	cell	23	4.2	650	9.9	64.0	0.97	N719+SDA	1.82
170	Colonna, D. <i>et al.</i>	⁸¹	dye sensitized PV	st, nws	cell	23	3.6	650	8.2	68.0	0.83	N719	2.01
171	Chalkias, D. A. <i>et al.</i>	⁸³	dye sensitized PV	st, ws	cell	24	7.8	794	17.4	56.3	1.87	N719 (EtOH)	2.00
172	Colonna, D. <i>et al.</i>	⁸¹	dye sensitized PV	st, nws	cell	25	2.6	650	5.6	71.0	0.65	N719+SDA	1.82
173	Huaulmé, Q. <i>et al.</i>	⁸⁴	dye sensitized PV	st, ws	cell	27	3.7	521	10.7	65.8	1.00	NPI	1.77
174	Colonna, D. <i>et al.</i>	⁸¹	dye sensitized PV	st, nws	cell	30	1.5	640	3.3	70.0	0.45	N719	2.19
175	Chalkias, D. A. <i>et al.</i>	⁸³	dye sensitized PV	st, ws	cell	31	6.4	698	13.5	67.9	1.98	TPA-1 (EtOH)	2.23
176	Chalkias, D. A. <i>et al.</i>	⁸³	dye sensitized PV	st, ws	cell	33	6.1	711	12.5	68.3	2.01	TPA-2 (EtOH)	2.3
177	Chalkias, D. A. <i>et al.</i>	⁸³	dye sensitized PV	st, ws	cell	36	6.1	766	14.5	54.7	2.20	TPA-1 (EtOH)	2.23
178	Chalkias, D. A. <i>et al.</i>	⁸⁵	dye sensitized PV	st, ws	cell	37	3.5	648	8.0	67.5	1.30	Cz-2	2.46
179	Chalkias, D. A. <i>et al.</i>	⁸³	dye sensitized PV	st, ws	cell	38	5.7	769	13.6	54.2	2.17	TPA-2 (EtOH)	2.31
180	Kim, K. <i>et al.</i>	⁸⁶	dye sensitized PV	st, nws	cell	43	7.8	720	15.3	70.8	3.35	PdTPBP/BPEA	1.95
181	Naim, W. <i>et al.</i>	⁸⁷	dye sensitized PV	st, ws	cell	69	3.1	422	11.2	65.6	2.14	VG20-C ₁₆	1.39
182	Naim, W. <i>et al.</i>	⁸⁷	dye sensitized PV	st, ws	cell	76	2.3	406	8.6	65.9	1.75	VG20-C ₁₆	1.41

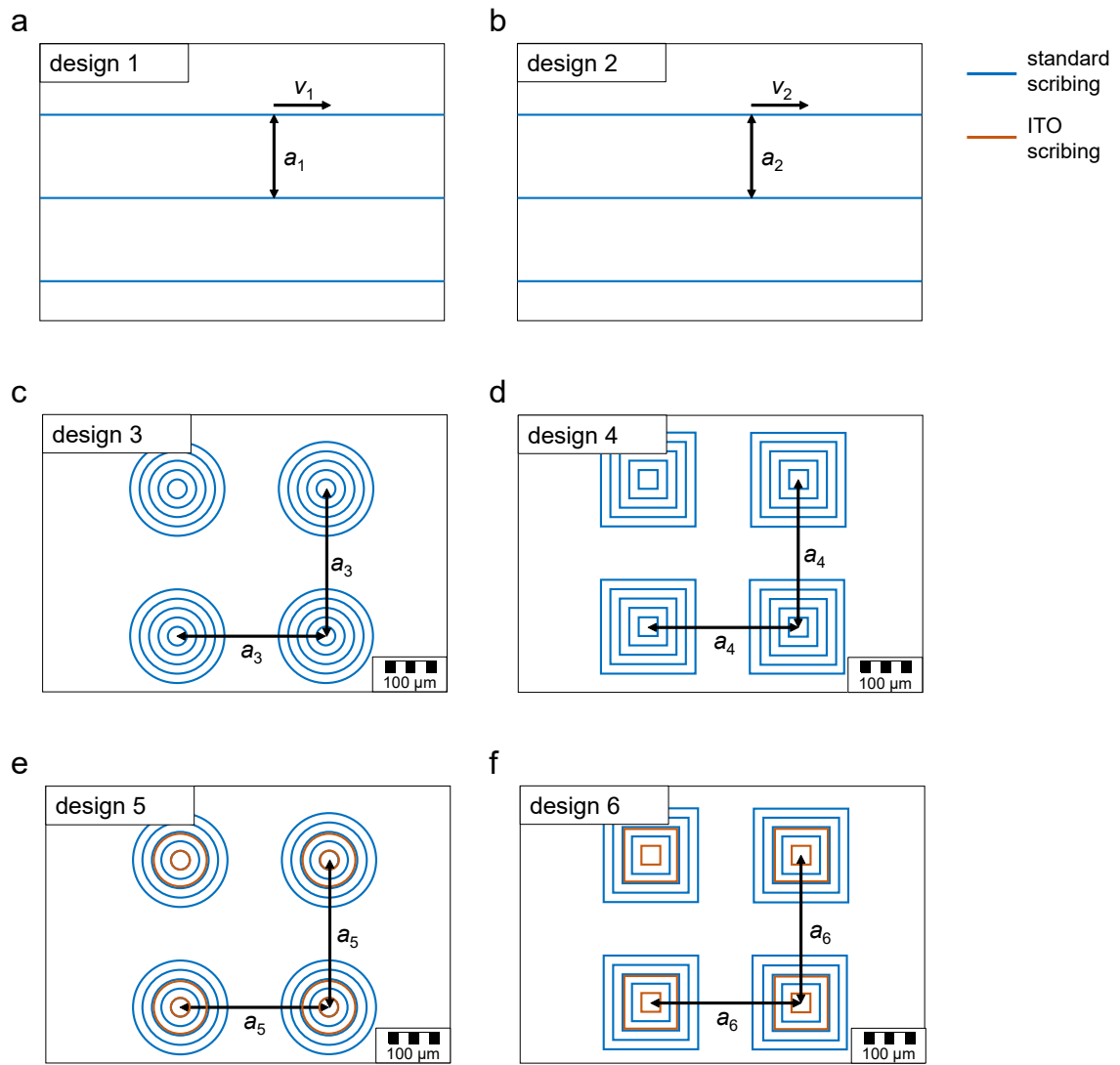


Figure S2. Laser scribing layouts for fabrication of transparent areas of various shapes. a) Scribing layout for design 1 – small circular transparent areas. b) Scribing layout for design 2 – transparent areas in shape of stripes. c) Scribing layout for design 3 – large circular transparent areas. d) Scribing layout for design 4 – square transparent areas. e) Scribing layout for design 5 – large circular transparent areas with ITO ablation. f) Scribing layout for design 6 – square transparent areas with ITO ablation. To obtain the desired AVT of translucent areas of devices, scribing velocity v_1 as well as spacing of scribing lines/circles/squares a_1-a_6 are calculated via a developed MATLAB scripts. Standard scribing velocity v_2 for design 2-6 is 100 mm/s. ITO scribing velocity is 100 mm/s.

Figure S3. Measured transmittance spectra and resulting optical parameters for a standard glass substrate of 1.1 mm thickness and a standard glass substrate with deposited indium tin oxide (ITO) as transparent front contact. Average visible transmittance (AVT), color rendering index (CRI) and CIELAB chromaticity coordinates (L^* , a^* , b^*) are calculated as discussed in the manuscript.

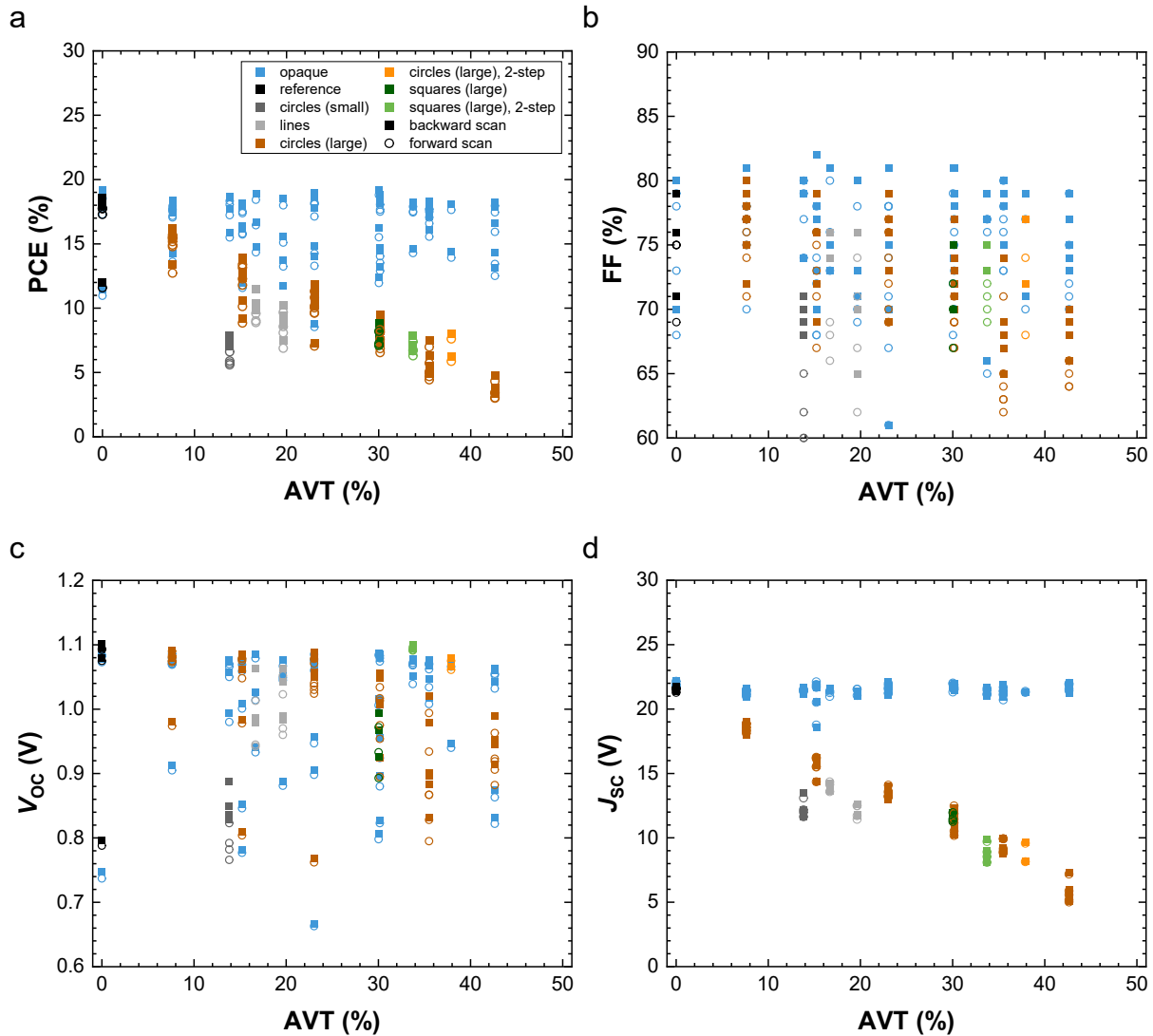


Figure S4. Statistical comparison of photovoltaic parameters (a) PCE, (b) FF, (c) V_{oc} , and (d) J_{sc} of perovskite solar cells before (opaque) and after fabrication of laser scribed transparent areas. Parameters are extracted from $J-V$ measurements in forward and backward scan direction. Statistics are based on 4 reference and 58 translucent solar cells with 0.105 cm^2 aperture area.

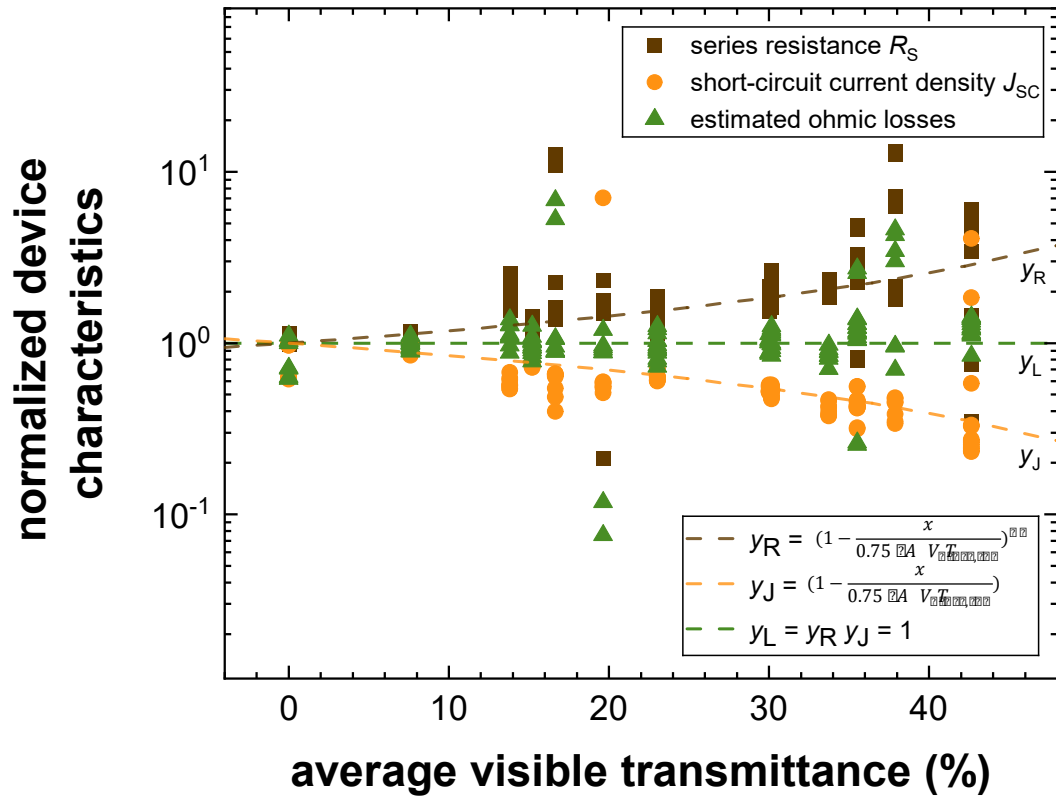


Figure S5. Analysis of the effect of laser scribing transparent areas in perovskite solar cells on series resistance R_S , short-circuit current density J_{SC} and resulting ohmic losses. Dashed lines depict the trend of respective characteristic for AVTs of devices of up to 35%. The factor of 0.75 used in the formulae for plotting the trends is stating the discrepancy between theoretical optimum and observed AVTs for given introduction of inactive areas as shown in Figure 2b of the manuscript. For AVTs above 35%, an over-proportional increase in series resistance is resulting in significantly increased ohmic losses.

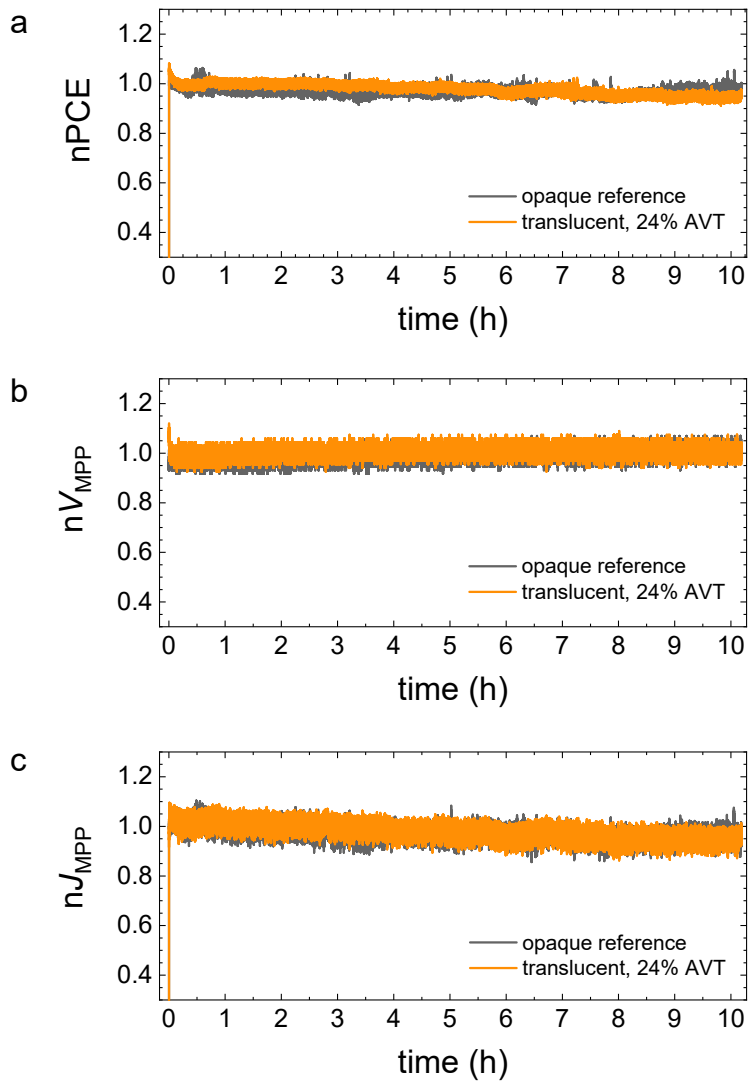


Figure S6. Assessment of short-term stability of translucent perovskite solar cells as introduced in chapter 2.1 in the manuscript. A translucent perovskite solar cell with intermediate transmittance level as well as an opaque reference solar cell were measured for more than 10 h under constant illumination (maximum power point tracking at nominal operating cell temperature). The results indicate no immediate or accelerated degradation induced by the laser scribing process, as (a) normalized PCE, (b) normalized voltage at MPP and (c) normalized current-density at MPP demonstrate a stable and very similar behavior.

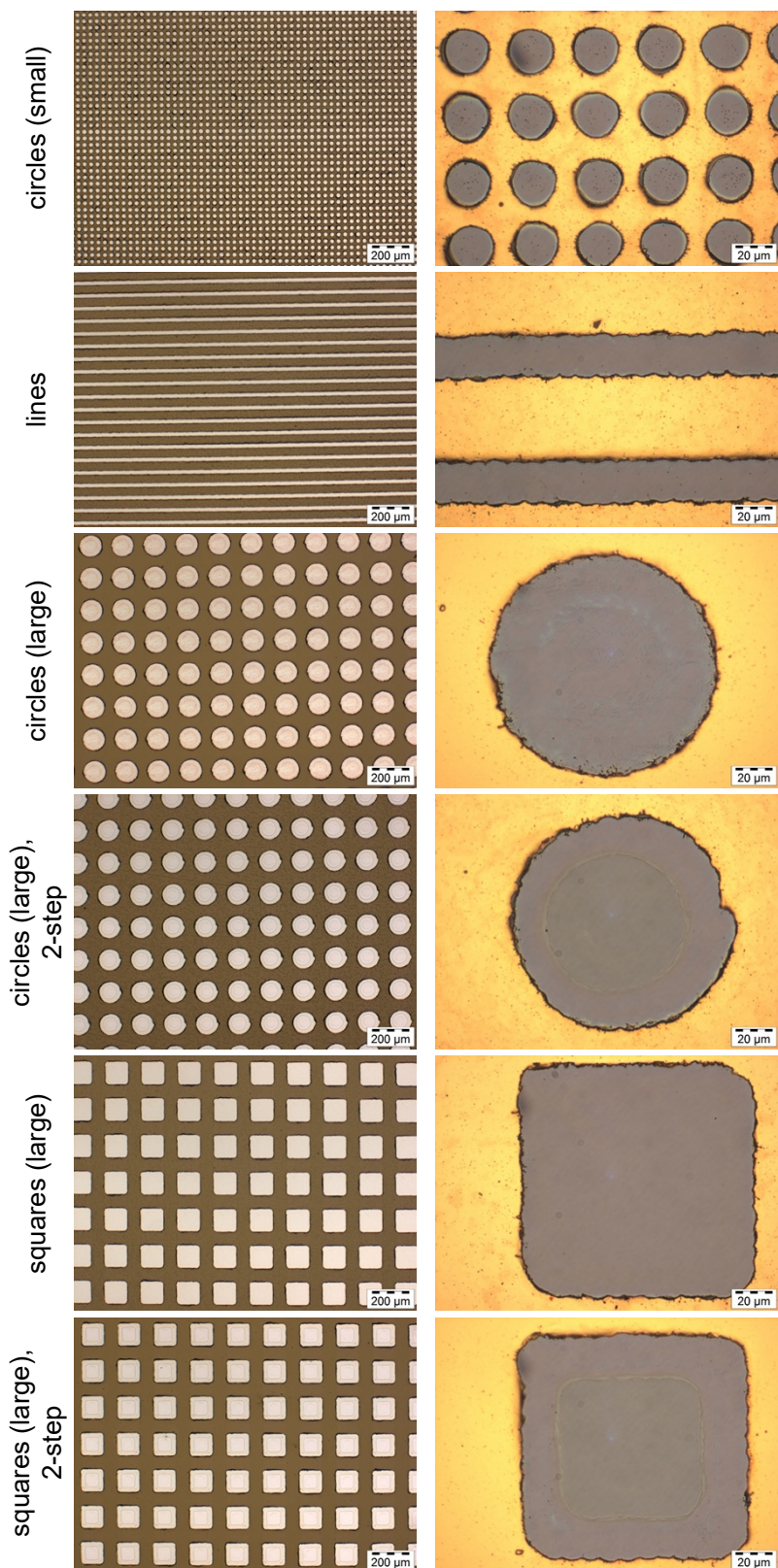


Figure S7. Light microscopy images at different magnifications (horizontal) of opaque perovskite solar modules with laser scribed transparent areas of different shapes (vertical).

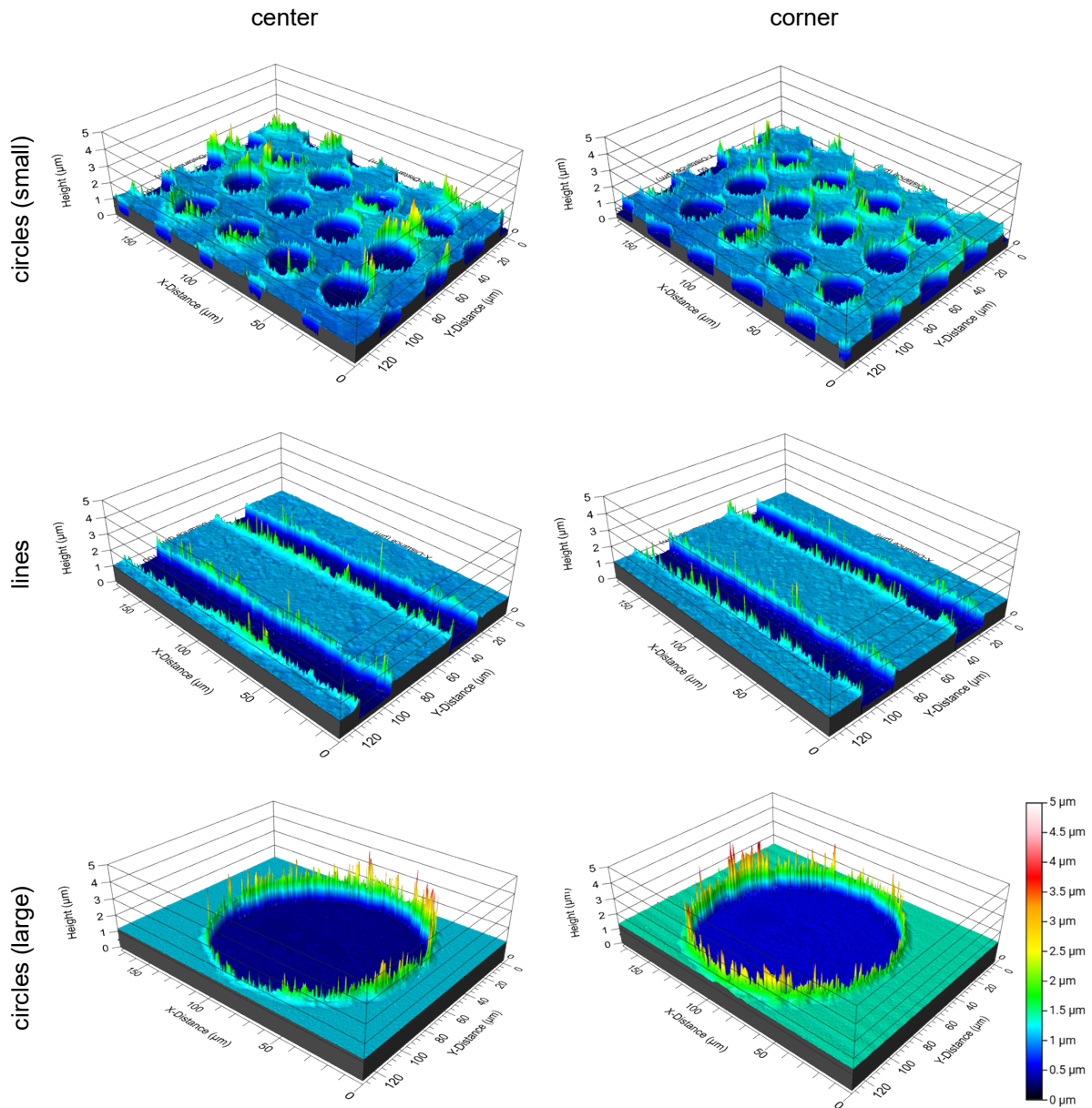


Figure S8. (Part a) Vertical scanning interferometry analysis of perovskite solar modules with laser scribed transparent areas of different shapes. Shown data demonstrates that transparent areas are free of residues. Furthermore, the flake formation of the metal back contact layer is mitigated and only minimal upward bending at the crater edges can be observed. Transparent areas with additional ITO ablation via 2-step approach show a homogeneous and thorough centric removal of ITO and no detrimental effect on crater edge areas. It should be noted that the sharp peaks are measurements artifacts caused by the “batwing effect” and do not represent actual defects. These batwing artifacts appear for interferometry measurements when the height difference (e.g. for sharp edges) are smaller than the coherence length of utilized light source.⁸⁸

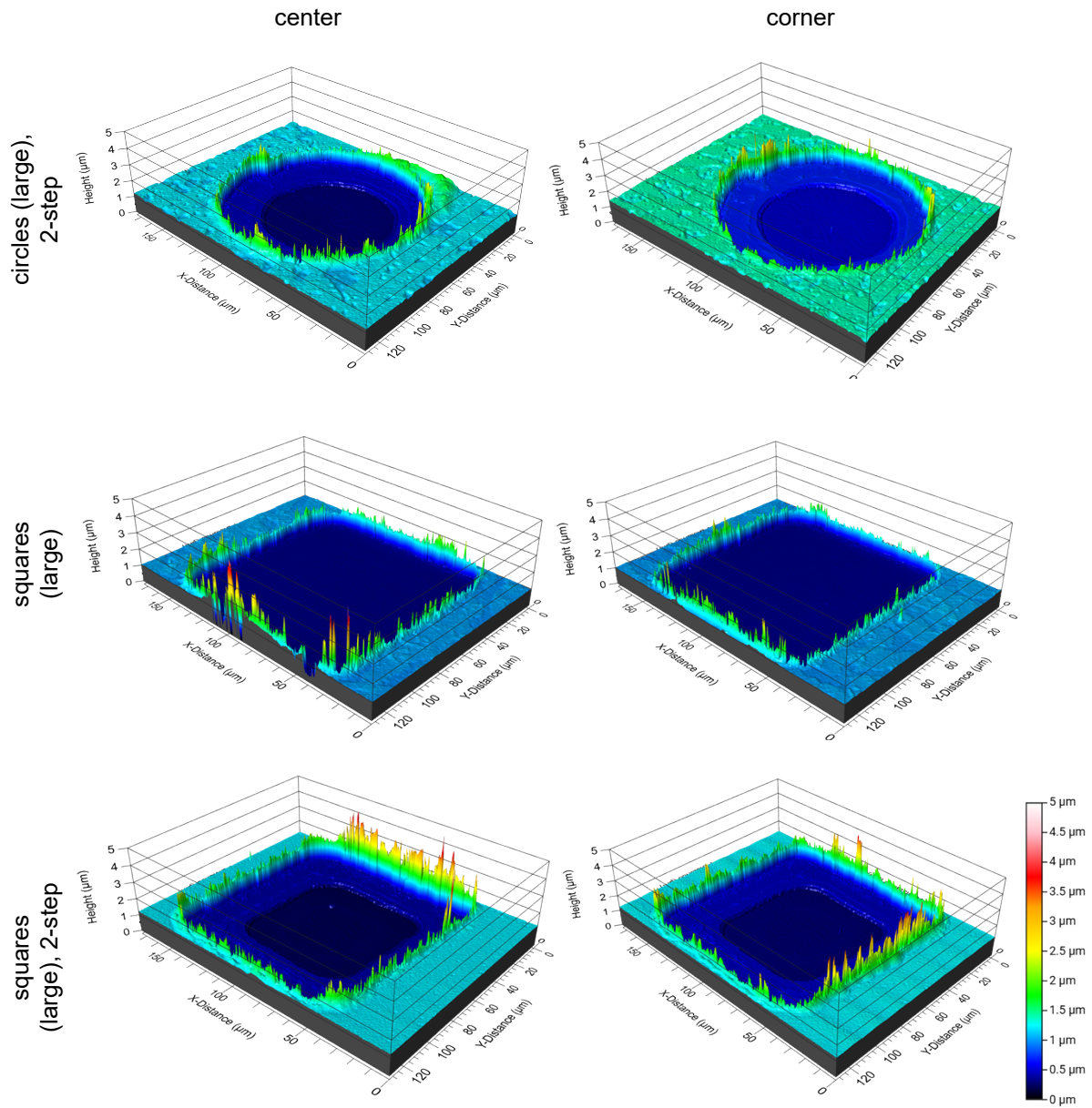
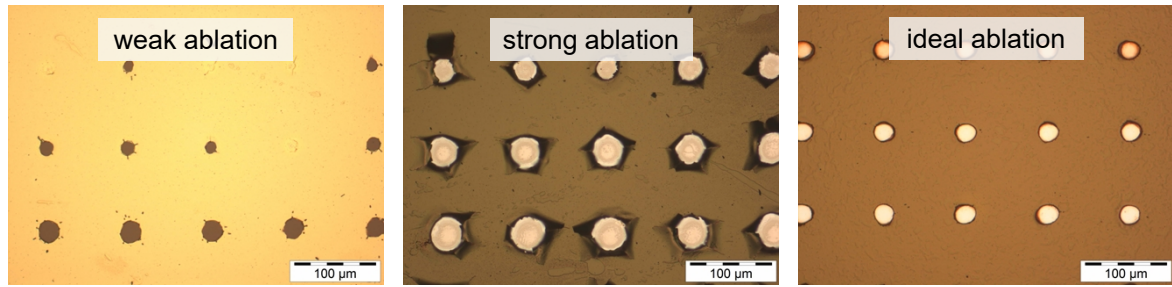
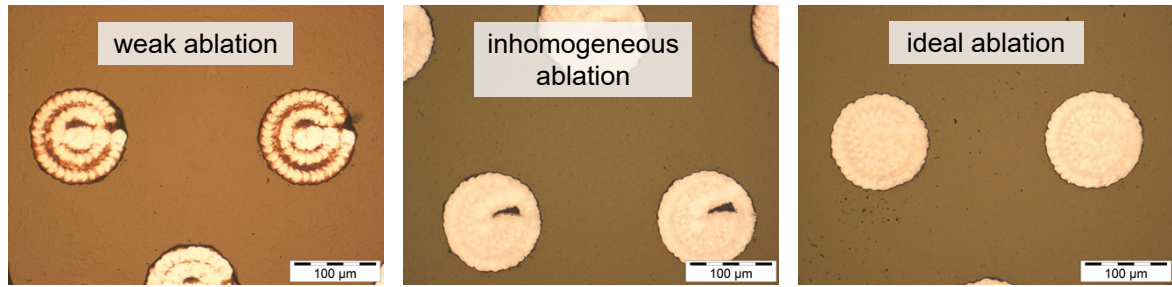


Figure S8. (Part b) Vertical scanning interferometry analysis of perovskite solar modules with laser scribed transparent areas of different shapes. Shown data demonstrates that transparent areas are free of residues. Furthermore, the flake formation of the back contact layer is mitigated and only minimal upward bending at the crater edges can be observed. Transparent areas with additional ITO ablation via 2-step approach show a homogeneous and thorough centric removal of ITO and no detrimental effect on crater edge areas. It should be noted that the sharp peaks are measurements artifacts caused by the “batwing effect” and do not represent actual defects. These batwing artifacts appear for interferometry measurements when the height difference (e.g. for sharp edges) are smaller than the coherence length of utilized light source.⁸⁸

a



b



c

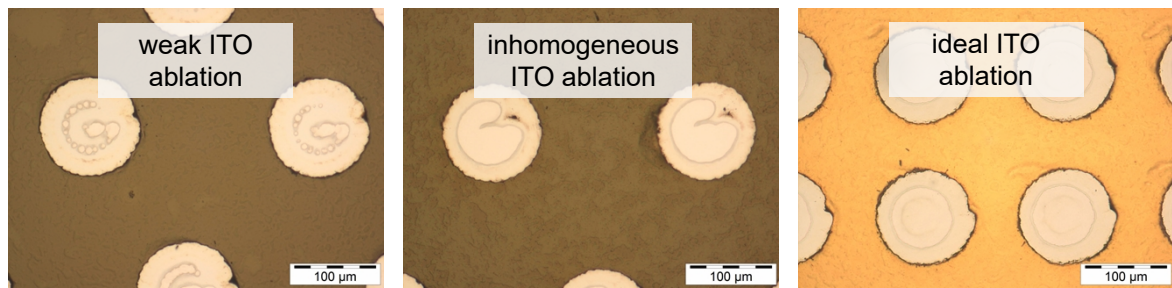


Figure S9. Exemplary presentation of parameter and design optimization for ideal laser scribing of transparent areas in perovskite solar cells and submodules. Small circular transparent areas (a) are fabricated with insufficient laser fluence (left) resulting in incomplete ablation, with too high laser fluence (middle) leading to strong detrimental flake formation and optimal laser fluence (right). Large circular transparent areas (b) and with additional centric front contact ablation (c) show fabrication results for insufficient laser fluence (left), for spatially-inhomogeneous laser pulsing (middle) due to incompatibility of lasing on-/off delays and scanner jump speed, and for optimized parameter sets (right). Optimization can require the adaption of laser fluence, scribing speed, lasing on-/off-delays, scanner jump speed, laser scribing layouts and back contact properties.

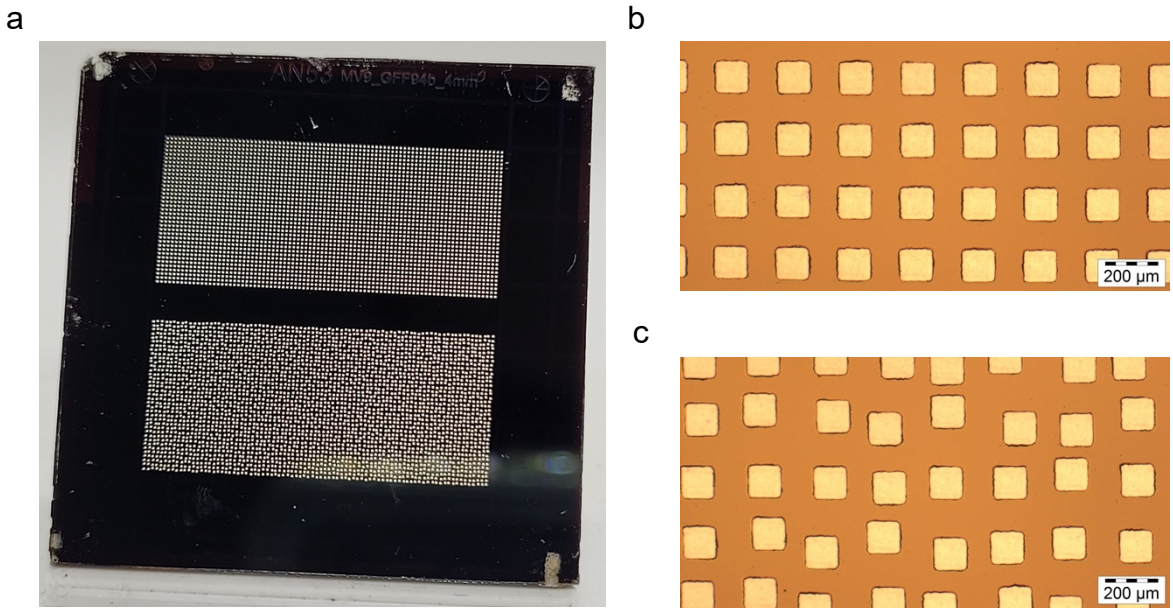


Figure S10. Illustration of the moiré effect, observable for images of translucent areas due to the superposition of two periodic structures (i.e. array of transparent areas and pixel-based monitors as display). a) Front side image of a translucent submodules with a periodic array of transparent areas (top) and spatially randomized transparent areas (bottom). The appearance of a visual pattern based on the moiré effect is significantly mitigated by the spatial randomization of transparent areas. Microscope images of the periodic array (b) and of the spatially randomized transparent areas (c).

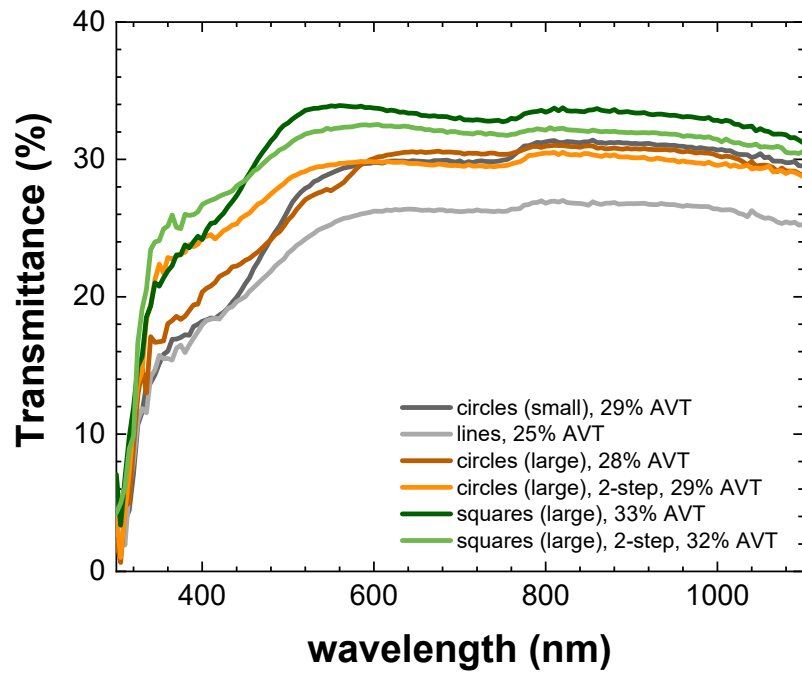


Figure S11. Transmittance spectra of translucent perovskite-based solar submodules with different transparent area formats as introduced in the manuscript on page 6 and 7, and in Figure 3.

Table S2. Optical parameters of translucent perovskite solar cell layer stacks with 4 cm² aperture area before and after fabrication of laser scribed transparent areas. The study focused on optical parameters to quantify the perceptual quality of fabricated translucent areas. The graphs of figure 3b and 3c in the manuscript are based on this data set.

substrate number	transparent area shape	AVT _{total} (%)	CRI	L*	a*	b*	AVT _{diffuse} (%)	AVT _{specular} AVT _{total} ⁻¹ (%)
1	circles (small)	29	92.2	59.5	1.9	11.7	4.4	84.5
2	lines	25	93.3	56.2	0.5	8.3	1.6	93.6
3	circles (large)	28	91.7	59.1	0.9	8.6	2.0	93.0
4	circles (large), 2-step	29	96.9	60.2	1.1	5.0	1.5	95.0
5	squares (large)	33	96.5	63.6	2.4	6.5	0.9	97.4
6	squares (large), 2-step	32	97.2	62.4	1.1	4.7	1.0	96.8

Table S3. Optical and photovoltaic parameters of the translucent perovskite submodule with 4 cm² aperture area before and after fabrication of laser scribed transparent areas, as presented in figure 4 in the manuscript. Regarding photovoltaic parameters, J-V characteristics of backward scans and forward scans (in brackets) are reported.

						before scribing				after scribing				comparison	
transparent area shape	AVT _{total} (%)	CRI	L*	a*	b*	PCE (%)	FF (%)	V _{oc} (V)	J _{sc} (mA cm ⁻²)	PCE (%)	FF (%)	V _{oc} (V)	J _{sc} (mA cm ⁻²)	relative PCE loss (%)	process efficiency (%)
squares (large), 2-step	32	95.1	62.5	0.6	5.0	15.2 (13.2)	69 (66)	5.54 (5.52)	19.91 (19.71)	9.0 (8.3)	74 (70)	5.50 (5.40)	11.11 (11.01)	40.8 (42.4)	78.9 (75.9)

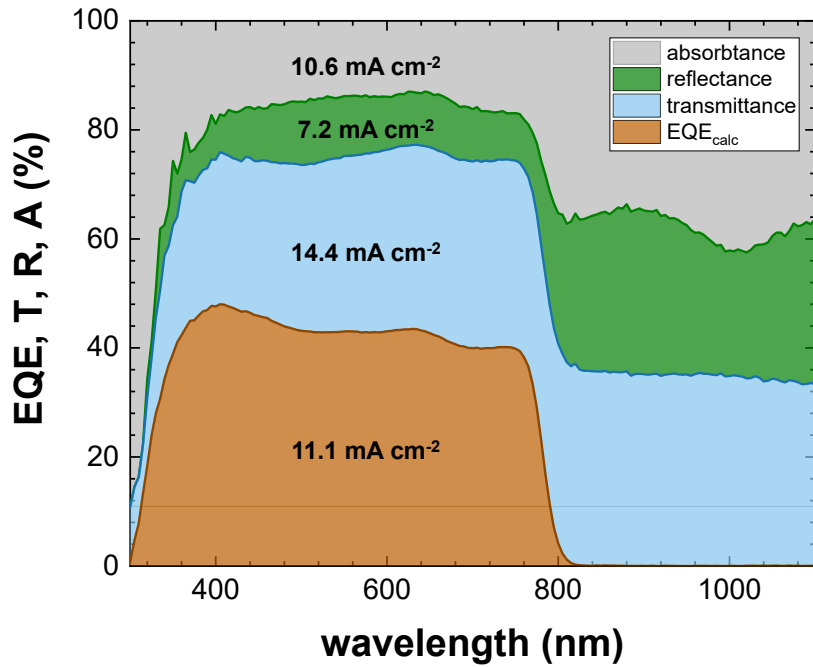


Figure S12. Photon balance consistency check of the translucent perovskite submodule, as presented in figure 4 of the manuscript. The presented EQE spectra is measured with a reference solar cell fabricated in the same batch and adapted to the measured current-density of the translucent submodule.

Table S4. Optical and photovoltaic parameters of the translucent 2-terminal perovskite-perovskite tandem solar cells with 8.1 mm² aperture area before and after fabrication of laser scribed transparent areas, as presented in figure 5 in the manuscript. Regarding photovoltaic parameters, *J-V* characteristics of backward scans and forward scans (in brackets) are reported.

						before scribing				after scribing				comparison	
transparent area shape	AVT _{total} (%)	CRI	L*	a*	b*	PCE (%)	FF (%)	V _{oc} (V)	J _{sc} (mA cm ⁻²)	PCE (%)	FF (%)	V _{oc} (V)	J _{sc} (mA cm ⁻²)	relative PCE loss (%)	process efficiency (%)
squares (large), 2-step	12	95.1	39.5	0.5	3.4	20.7 (17.3)	75 (64)	1.94 (1.93)	14.33 (13.93)	17.7 (15.0)	77 (68)	1.95 (1.94)	11.85 (11.36)	14.5 (13.3)	79.3 (86.2)
squares (large), 2-step	31	95.5	61.3	0.6	4.4	18.4 (15.2)	73 (64)	1.94 (1.93)	13.01 (12.37)	11.1 (9.3)	71 (61)	1.94 (1.94)	8.10 (7.85)	39.7 (38.8)	77.3 (79.1)

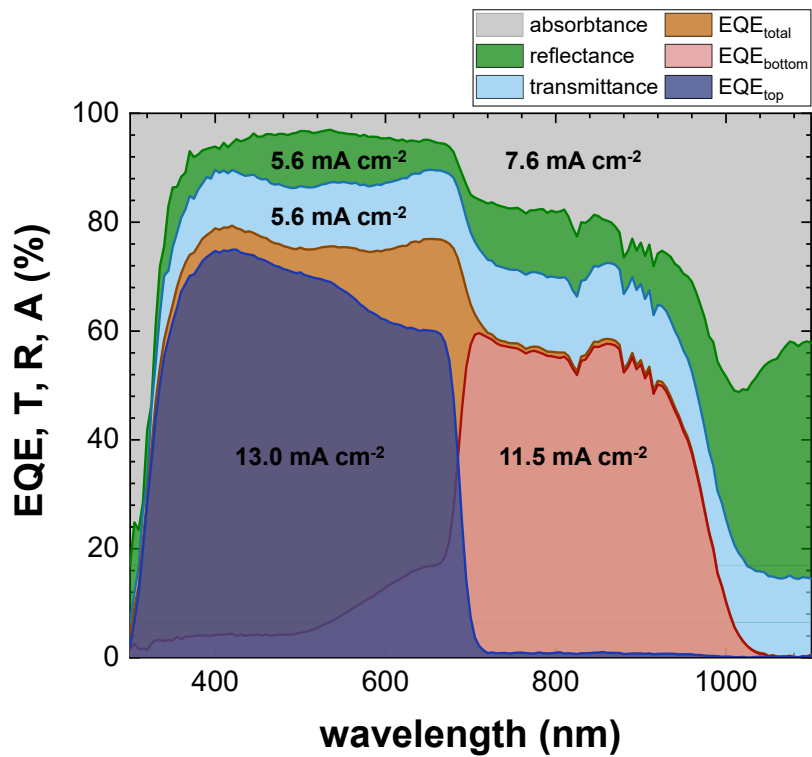


Figure S13. Photon balance consistency check of the translucent perovskite-perovskite tandem solar cell, as presented in figure 5b of the manuscript.

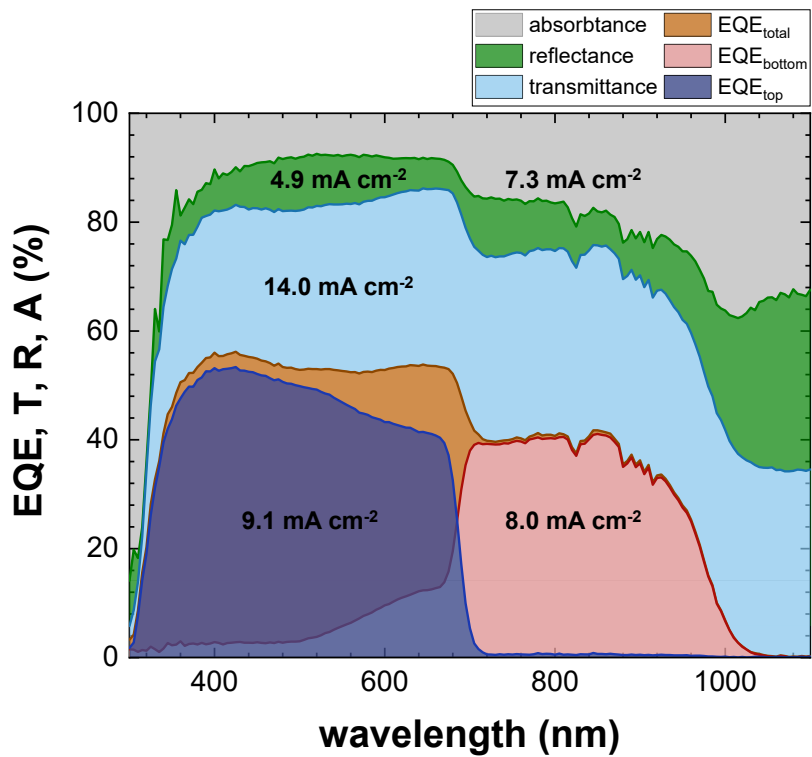


Figure S14. Photon balance consistency check of the translucent perovskite-perovskite tandem solar cell, as presented in figure 5c of the manuscript.

Table S5. Optical and photovoltaic parameters of the translucent 2-terminal perovskite-perovskite mini-module with 12.25 cm² aperture area before and after fabrication of laser scribed transparent areas, as presented in the manuscript. Regarding photovoltaic parameters, J-V characteristics of backward scans and forward scans (in brackets) are reported. Layer fabrication followed the recipe reported in our previous work.¹

						before scribing				after scribing				comparison	
transparent area shape	AVT _{total} (%)	CRI	L*	a*	b*	PCE (%)	FF (%)	V _{oc} (V)	J _{sc} (mA cm ⁻²)	PCE (%)	FF (%)	V _{oc} (V)	J _{sc} (mA cm ⁻²)	relative PCE loss (%)	process efficiency (%)
squares (large), 2-step	15	79.4	44.7	1.6	18.3	16.7 (14.0)	73 (64)	13.15 (13.06)	12.18 (11.76)	10.3 (8.9)	68 (61)	12.72 (12.73)	8.33 (8.11)	38.3 (36.4)	39.2 (41.2)

Figure S15. J-V characteristics of a translucent 2-terminal perovskite-perovskite tandem mini-module with 12.25 cm² aperture area, before (opaque) and after (translucent) fabrication of transparent areas at 12% AVT.

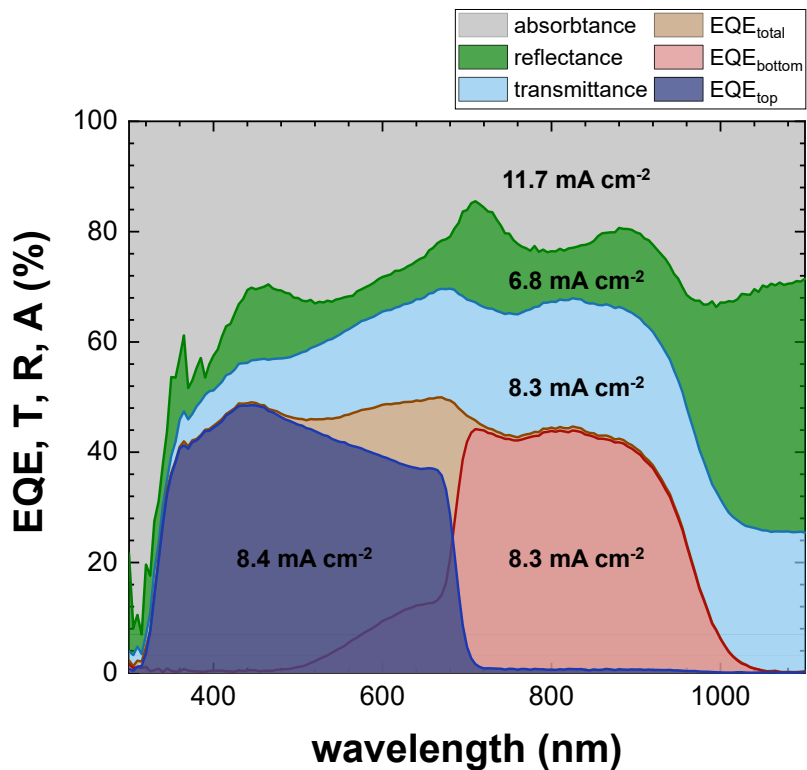


Figure S16. Photon balance consistency check of the translucent perovskite-perovskite tandem mini-module with 12.25 cm^2 aperture area, as presented in the manuscript. The EQE spectra of top and bottom sub-cell is measured with a reference tandem solar cell and adapted to the measured current-density of the translucent tandem mini-module.

$$r_{\text{t}} \approx \frac{A}{\eta A} \frac{V T l}{v_s s}$$

$$l_{\text{t}} \sim l_{\text{s}}$$

$$v_s \sim r_{\text{t}}(d_{\text{t}} - d_{\text{s}})$$

$$r_{\text{t},\text{c}} \approx \frac{0.3}{0.8 \cdot (0.012 \text{ c})} \frac{\pi \cdot 0.03 \text{ c}}{10 \text{ c}} \frac{m}{m^2} = 24.5 \text{ s c}^{-1} m^{-2}$$

$$= 4090 \text{ m i m}^{-2}$$

Current manufacturing rate:
 → Utilization of described laser setup
 → Calculation for large circular transparent areas

$$r_{\text{t},\text{p}} \approx \frac{0.3}{0.8 \cdot (0.012 \text{ c})} \frac{\pi \cdot 0.022 \text{ c}}{4 \cdot 1500 \text{ c}} \frac{m}{m^2} = 0.03 \text{ s c}^{-1} m^{-2}$$

$$= 2.2 \text{ m i m}^{-2}$$

Possible improvements:
 → Utilization of 1 MHz pulsed laser (max ~10 MHz)
 → Utilization of 3 x 3 galvanometer scanners per m²
 → Reduction of line and pulse overlap ratio from 0.6 to 0.4

r_t :	Manufacturing rate of translucent area	s :	Number of parallel scanners
$A_{V:T}$:	Targeted average visible transmittance	l_o :	Overlap of adjacent scribing lines
η_t :	Transmittance efficiency of transparent areas	r_l :	Laser pulse rate
A_t :	Transparent area of respective design	d_a :	Diameter of pulse ablation crater
l_t :	Scribing length per transparent area	d_o :	Overlap of adjacent scribing pulses
v_l :	Scribing speed		

Equation S1. Estimation of the manufacturing rate of translucent areas considering variable levels of average visible transmittance, different scribing layouts and parameters, as well as the utilized setup components. The first calculation is based on conditions utilized for this work. We note that the current process is strongly limited by the laser pulse rate (10 kHz). Furthermore, decreasing the utilized overlap ratio of pulses and lines of 60% offers additional potential for increasing manufacturing rate. The second calculation takes possible improvements of the laser scribing process (overlap) and the adaption of components (1 MHz pulsed laser; 9 galvanometer scanner) into account. The resulting manufacturing time per squaremeter is assumed to be compatible with modern industrial PV manufacturing lines.

Table S6. Optical and photovoltaic parameters of the translucent submodules with 4 cm² aperture area and transmittance gradients before and after fabrication of laser scribed transparent areas, as presented in figure 6 in the manuscript. Regarding photovoltaic parameters, *J-V* characteristics of backward scans and forward scans (in brackets) are reported. All transparent areas were laser scribed in the shape of squares (large) and with the 2-step process.

							before scribing				after scribing				comparison
direction of transmittance gradient	spot	AVT _{total} (%)	CRI	L*	a*	b*	PCE (%)	FF (%)	V _{oc} (V)	J _{sc} (mA cm ⁻²)	PCE (%)	FF (%)	V _{oc} (V)	J _{sc} (mA cm ⁻²)	relative PCE loss (%)
horizontal	M1	31	94.9	61.7	0.8	4.8	16.0 (14.9)	72 (69)	5.61 (5.55)	19.76 (19.61)	12.0 (11.3)	74 (71)	5.58 (5.52)	11.61 (11.57)	25.0 (24.2)
	M2	7	90.6	31.3	0.8	3.5									
vertical	M1	33	96.4	63.0	0.3	4.0	13.3 (11.9)	76 (69)	5.49 (5.37)	15.98 (15.98)	10.3 (9.8)	66 (65)	5.39 (5.26)	11.57 (11.45)	22.6 (17.6)
	M2	5	88.0	25.0	2.1	4.2									
radial	M1	28	95.7	59.2	1.0	4.8	12.9 (11.9)	65 (61)	5.26 (5.17)	18.89 (18.84)	11.2 (10.2)	72 (68)	5.36 (5.17)	11.53 (11.65)	13.2 (14.3)
	M2	8	93.5	24.1	1.9	3.9									

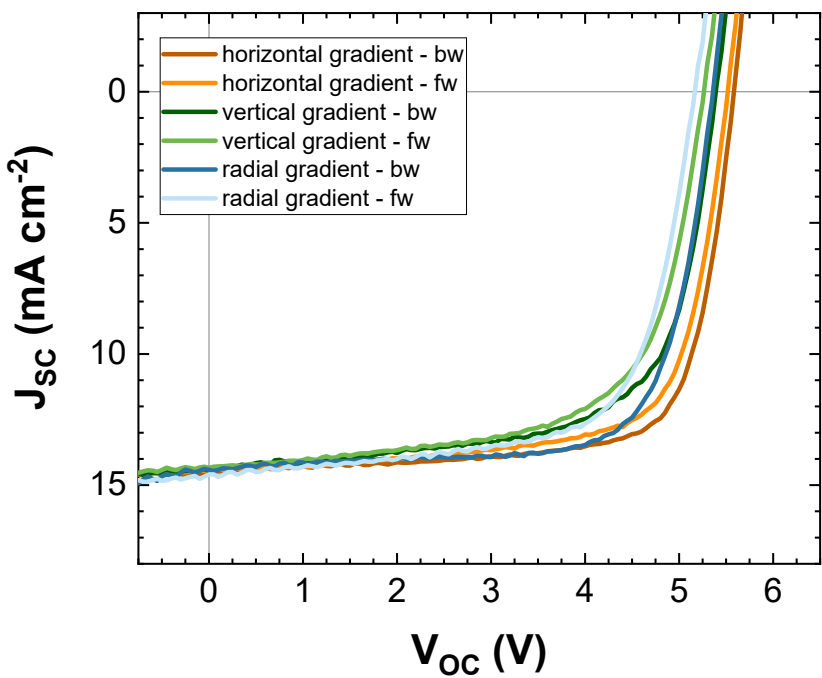


Figure S17. J - V characteristics of the translucent perovskite submodules with 4 cm^2 aperture area after fabrication of transmittance gradients, as presented in figure 6 in the manuscript.

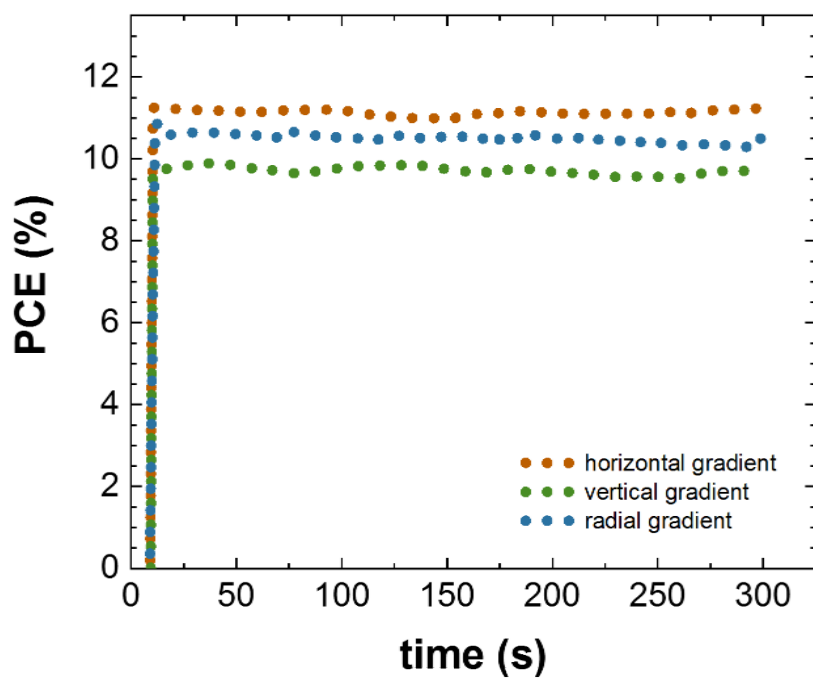


Figure S18. Short-term stability of the translucent perovskite submodules with 4 cm² aperture area after fabrication of transmittance gradients under continuous illumination during MPP tracking at nominal operating cell temperature (NOCT) conditions without active cooling.

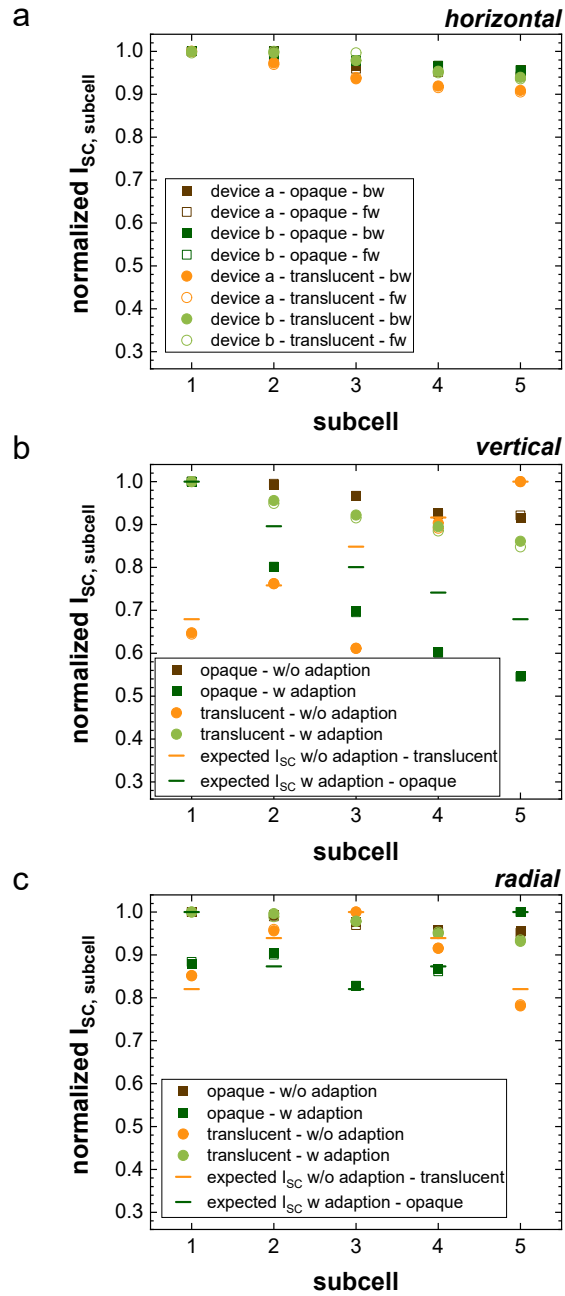


Figure S19. Comparison of normalized subcell currents before (opaque) and after (translucent) fabrication of transmittance gradients and without (w/o) and with (w) adaption of subcell width for current matching of subcells in the translucent perovskite submodules. a) The transmittance gradient is horizontal (in parallel to interconnection lines) and no current mismatch should occur. The only minimal higher current mismatch for translucent subcells than for opaque subcells demonstrates high homogeneity of fabricated transparent areas over the entire substrate area. b) The transmittance gradient is vertical (perpendicular to interconnection lines) and without adaption a current mismatch will occur. The much smaller current mismatch for translucent submodules with adapted cell widths demonstrates the feasibility of transmittance-related current-density estimations and subsequent design alterations for device optimization. c) The transmittance gradient has its origin in the center of the substrate, proceeds radially to the substrate edges and will generate a current mismatch without adaptions. The much smaller current mismatch for translucent submodules with adapted cell widths further confirms the feasibility of device optimizations via design alterations.

References

1. Nejand, B.A., Ritzer, D.B., Hu, H., Schackmar, F., Moghadamzadeh, S., Feeney, T., Singh, R., Laufer, F., Schmager, R., Azmi, R., et al. (2022). Scalable two-terminal all-perovskite tandem solar modules with a 19.1% efficiency. *Nat. Energy* **7**, 620–630. 10.1038/s41560-022-01059-w.
2. Ritzer, D.B., Abzieher, T., Basibüyük, A., Feeney, T., Laufer, F., Ternes, S., Richards, B.S., Bergfeld, S., and Paetzold, U.W. (2022). Upscaling of perovskite solar modules: The synergy of fully evaporated layer fabrication and all-laser-scribed interconnections. *Prog. Photovoltaics Res. Appl.* **30**, 360–373. 10.1002/pip.3489.
3. Yang, C., Liu, D., Bates, M., Barr, M.C., and Lunt, R.R. (2019). How to Accurately Report Transparent Solar Cells. *Joule* **3**, 1803–1809. 10.1016/j.joule.2019.06.005.
4. Almora, O., Baran, D., Bazan, G.C., Berger, C., Cabrera, C.I., Catchpole, K.R., Erten-Ela, S., Guo, F., Hauch, J., Ho-Baillie, A.W.Y., et al. (2021). Device Performance of Emerging Photovoltaic Materials (Version 1). *Adv. Energy Mater.* **11**. 10.1002/aenm.202002774.
5. Lim, S.H., Seok, H.J., Kwak, M.J., Choi, D.H., Kim, S.K., Kim, D.H., and Kim, H.K. (2021). Semi-transparent perovskite solar cells with bidirectional transparent electrodes. *Nano Energy* **82**, 105703. 10.1016/j.nanoen.2020.105703.
6. Li, C., Sleppy, J., Dhasmana, N., Soliman, M., Tetard, L., and Thomas, J. (2016). A PCBM-assisted perovskite growth process to fabricate high efficiency semitransparent solar cells. *J. Mater. Chem. A* **4**, 11648–11655. 10.1039/c6ta04790d.
7. Ying, Z., Yang, X., Zheng, J., Zhu, Y., Xiu, J., Chen, W., Shou, C., Sheng, J., Zeng, Y., Yan, B., et al. (2021). Charge-transfer induced multifunctional BCP:Ag complexes for semi-transparent perovskite solar cells with a record fill factor of 80.1%. *J. Mater. Chem. A* **9**, 12009–12018. 10.1039/d1ta01180d.
8. Chen, B., Bai, Y., Yu, Z., Li, T., Zheng, X., Dong, Q., Shen, L., Boccard, M., Gruverman, A., Holman, Z., et al. (2016). Efficient Semitransparent Perovskite Solar Cells for 23.0%-Efficiency Perovskite/Silicon Four-Terminal Tandem Cells. *Adv. Energy Mater.* **6**. 10.1002/aenm.201601128.
9. You, P., Liu, Z., Tai, Q., Liu, S., and Yan, F. (2015). Efficient Semitransparent Perovskite Solar Cells with Graphene Electrodes. *Adv. Mater.* **27**, 3632–3638. 10.1002/adma.201501145.
10. Jang, C.W., Kim, J.M., and Choi, S.H. (2019). Lamination-produced semi-transparent/flexible perovskite solar cells with doped-graphene anode and cathode. *J. Alloys Compd.* **775**, 905–911. 10.1016/j.jallcom.2018.10.190.
11. Heo, J.H., Han, H.J., Lee, M., Song, M., Kim, D.H., and Im, S.H. (2015). Stable semi-transparent CH₃NH₃PbI₃ planar sandwich solar cells. *Energy Environ. Sci.* **8**, 2922–2927. 10.1039/c5ee01050k.
12. Della Gaspera, E., Peng, Y., Hou, Q., Spiccia, L., Bach, U., Jasieniak, J.J., and Cheng, Y.B. (2015). Ultra-thin high efficiency semitransparent perovskite solar cells. *Nano Energy* **13**, 249–257. 10.1016/j.nanoen.2015.02.028.
13. Eperon, G.E., Burlakov, V.M., Goriely, A., and Snaith, H.J. (2014). Neutral color semitransparent microstructured perovskite solar cells. *ACS Nano* **8**, 591–598. 10.1021/nn4052309.
14. Rakocevic, L., Gehlhaar, R., Jaysankar, M., Song, W., Aernouts, T., Fledderus, H., and Poortmans, J. (2018). Translucent, color-neutral and efficient perovskite thin film solar modules. *J. Mater. Chem. C* **6**, 3034–3041. 10.1039/c7tc05863b.

15. Yang, D., Zhang, X., Hou, Y., Wang, K., Ye, T., Yoon, J., Wu, C., Sanghadasa, M., Liu, S. (Frank), and Priya, S. (2021). 28.3%-Efficiency Perovskite/Silicon Tandem Solar Cell By Optimal Transparent Electrode for High Efficient Semitransparent Top Cell. *Nano Energy* 84, 105934. 10.1016/j.nanoen.2021.105934.
16. Yuan, L., Wang, Z., Duan, R., Huang, P., Zhang, K., Chen, Q., Allam, N.K., Zhou, Y., Song, B., and Li, Y. (2018). Semi-transparent perovskite solar cells: Unveiling the trade-off between transparency and efficiency. *J. Mater. Chem. A* 6, 19696–19702. 10.1039/c8ta07318j.
17. Yu, J.C., Sun, J., Chandrasekaran, N., Dunn, C.J., Chesman, A.S.R., and Jasieniak, J.J. (2020). Semi-transparent perovskite solar cells with a cross-linked hole transport layer. *Nano Energy* 71, 104635. 10.1016/j.nanoen.2020.104635.
18. Ramírez Quiroz, C.O., Levchuk, I., Bronnbauer, C., Salvador, M., Forberich, K., Heumüller, T., Hou, Y., Schweizer, P., Spiecker, E., and Brabec, C.J. (2015). Pushing efficiency limits for semitransparent perovskite solar cells. *J. Mater. Chem. A* 3, 24071–24081. 10.1039/c5ta08450d.
19. Zhang, Y.W., Cheng, P.P., Tan, W.Y., and Min, Y. (2021). Balance the thickness, transparency and stability of semi-transparent perovskite solar cells by solvent engineering and using a bifunctional additive. *Appl. Surf. Sci.* 537, 147908. 10.1016/j.apsusc.2020.147908.
20. Dou, Y., Liu, Z., Wu, Z., Liu, Y., Li, J., Leng, C., Fang, D., Liang, G., Xiao, J., Li, W., et al. (2020). Self-augmented ion blocking of sandwiched 2D/1D/2D electrode for solution processed high efficiency semitransparent perovskite solar cell. *Nano Energy* 71, 104567. 10.1016/j.nanoen.2020.104567.
21. Xiao, S., Chen, H., Jiang, F., Bai, Y., Zhu, Z., Zhang, T., Zheng, X., Qian, G., Hu, C., Zhou, Y., et al. (2016). Hierarchical Dual-Scaffolds Enhance Charge Separation and Collection for High Efficiency Semitransparent Perovskite Solar Cells. *Adv. Mater. Interfaces* 3.
22. Chang, C.Y., Lee, K.T., Huang, W.K., Siao, H.Y., and Chang, Y.C. (2015). High-Performance, Air-Stable, Low-Temperature Processed Semitransparent Perovskite Solar Cells Enabled by Atomic Layer Deposition. *Chem. Mater.* 27, 5122–5130. 10.1021/acs.chemmater.5b01933.
23. Jung, J.W., Chueh, C.-C., and Jen, A.K.-Y. (2015). High-Performance Semitransparent Perovskite Solar Cells with 10% Power Conversion Efficiency and 25% Average Visible Transmittance Based on Transparent CuSCN as the Hole-Transporting Material. *Adv. Energy Mater.* 5. 10.1002/aenm.201500486.
24. Guo, F., Azimi, H., Hou, Y., Przybilla, T., Hu, M., Bronnbauer, C., Langner, S., Spiecker, E., Forberich, K., and Brabec, C.J. (2015). High-performance semitransparent perovskite solar cells with solution-processed silver nanowires as top electrodes. *Nanoscale* 7, 1642–1649. 10.1039/c4nr06033d.
25. Eperon, G.E., Bryant, D., Troughton, J., Stranks, S.D., Johnston, M.B., Watson, T., Worsley, D.A., and Snaith, H.J. (2015). Efficient, semitransparent neutral-colored solar cells based on microstructured formamidinium lead trihalide perovskite. *J. Phys. Chem. Lett.* 6, 129–138. 10.1021/jz502367k.
26. Kwon, H.C., Kim, A., Lee, H., Lee, D., Jeong, S., and Moon, J. (2016). Parallelized Nanopillar Perovskites for Semitransparent Solar Cells Using an Anodized Aluminum Oxide Scaffold. *Adv. Energy Mater.* 6. 10.1002/aenm.201601055.
27. Roldán-Carmona, C., Malinkiewicz, O., Betancur, R., Longo, G., Momblona, C., Jaramillo, F., Camacho, L., and Bolink, H.J. (2014). High efficiency single-junction semitransparent perovskite solar cells. *Energy Environ. Sci.* 7, 2968–2973. 10.1039/c4ee01389a.

28. Zhang, L., Hörantner, M.T., Zhang, W., Yan, Q., and Snaith, H.J. (2017). Near-neutral-colored semitransparent perovskite films using a combination of colloidal self-assembly and plasma etching. *Sol. Energy Mater. Sol. Cells* **160**, 193–202. 10.1016/j.solmat.2016.10.035.
29. Bag, S., and Durstock, M.F. (2016). Efficient semi-transparent planar perovskite solar cells using a ‘molecular glue.’ *Nano Energy* **30**, 542–548. 10.1016/j.nanoen.2016.10.044.
30. Liu, G., Wu, C., Zhang, Z., Chen, Z., Xiao, L., and Qu, B. (2020). Ultraviolet-Protective Transparent Photovoltaics Based on Lead-Free Double Perovskites.
31. Zuo, L., Shi, X., Fu, W., and Jen, A.K.Y. (2019). Highly Efficient Semitransparent Solar Cells with Selective Absorption and Tandem Architecture. *Adv. Mater.* **31**, 1–9. 10.1002/adma.201901683.
32. Liu, D., Yang, C., and Lunt, R.R. (2018). Halide Perovskites for Selective Ultraviolet-Harvesting Transparent Photovoltaics. *Joule* **2**, 1827–1837. 10.1016/j.joule.2018.06.004.
33. Shin, M.J., Jo, J.H., Cho, A., Gwak, J., Yun, J.H., Kim, K., Ahn, S.K., Park, J.H., Yoo, J., Jeong, I., et al. (2019). Semi-transparent photovoltaics using ultra-thin Cu(In,Ga)Se₂ absorber layers prepared by single-stage co-evaporation. *Sol. Energy* **181**, 276–284. 10.1016/j.solener.2019.02.003.
34. Shin, M.J., Park, S., Lee, A., Park, S.J., Cho, A., Kim, K., Ahn, S.K., Hyung Park, J., Yoo, J., Shin, D., et al. (2021). Bifacial photovoltaic performance of semitransparent ultrathin Cu(In,Ga)Se₂ solar cells with front and rear transparent conducting oxide contacts. *Appl. Surf. Sci.* **535**, 147732. 10.1016/j.apsusc.2020.147732.
35. Kim, J., Lim, J.W., Kim, G., and Shin, M. (2021). Effects of moisture-proof back passivation layers of Al₂O₃ and Al_xTi_{1-x}O_y films on efficiency improvement and color modulation in transparent a-Si:H solar cells. *ACS Appl. Mater. Interfaces* **13**, 4968–4974. 10.1021/acsami.0c17245.
36. Kim, K., and Shafarman, W.N. (2016). Alternative device structures for CIGS-based solar cells with semi-transparent absorbers. *Nano Energy* **30**, 488–493. 10.1016/j.nanoen.2016.10.038.
37. Schott Solar GmbH (2010). ASI THRU thin-film solar module, semitransparent.
38. Polysolar Limited (2022). PS-CT series panels.
39. Onyx Solar Group LLC (2022). Amorphous Silicon PV Glass.
40. Polysolar Limited (2021). PS-MC-ST Series panels.
41. Glaswerke Arnold GmbH & Co. KG (2011). VOLTARLUX ASI-Glas.
42. Kuk, S., Wang, Z., Yu, H., Nam, C.Y., Jeong, J. hyun, and Hwang, D. (2019). Nanosecond laser scribing for see-through CIGS thin film solar cells. *Prog. Photovoltaics Res. Appl.*, 135–147. 10.1002/pip.3219.
43. Yang, R., Lee, C.H., Cui, B., and Sazonov, A. (2018). Flexible semi-transparent a-Si:H pin solar cells for functional energy-harvesting applications. *Mater. Sci. Eng. B Solid-State Mater. Adv. Technol.* **229**, 1–5. 10.1016/j.mseb.2017.12.005.
44. Cho, J.S., Seo, Y.H., Choi, B.H., Cho, A., Lee, A., Shin, M.J., Kim, K., Ahn, S.K., Park, J.H., Yoo, J., et al. (2019). Energy harvesting performance of bifacial and semitransparent amorphous silicon thin-film solar cells with front and rear transparent conducting oxide contacts. *Sol. Energy Mater. Sol. Cells* **202**, 110078. 10.1016/j.solmat.2019.110078.
45. Lim, J.W., Lee, S.H., Lee, D.J., Lee, Y.J., and Yun, S.J. (2013). Performances of amorphous silicon and silicon germanium semi-transparent solar cells. *Thin Solid Films* **547**, 212–215. 10.1016/j.tsf.2013.03.038.

46. Saifullah, M., Ahn, S., Gwak, J., Ahn, S., Kim, K., Cho, J., Park, J.H., Eo, Y.J., Cho, A., Yoo, J.S., et al. (2016). Development of semitransparent CIGS thin-film solar cells modified with a sulfurized-AgGa layer for building applications. *J. Mater. Chem. A* **4**, 10542–10551. 10.1039/c6ta01909a.
47. Moon, S.H., Park, S.J., Hwang, Y.J., Lee, D.K., Cho, Y., Kim, D.W., and Min, B.K. (2014). Printable, wide band-gap chalcopyrite thin films for power generating window applications. *Sci. Rep.* **4**, 1–6. 10.1038/srep04408.
48. Tsai, C.Y., and Tsai, C.Y. (2020). See-through, light-through, and color modules for large-area tandem amorphous/microcrystalline silicon thin-film solar modules: Technology development and practical considerations for building-integrated photovoltaic applications. *Renew. Energy* **145**, 2637–2646. 10.1016/j.renene.2019.08.029.
49. Park, J., Lee, K., and Seo, K. (2022). 25-Cm² Glass-Like Transparent Crystalline Silicon Solar Cells With an Efficiency of 14.5%. *Cell Reports Phys. Sci.* **3**, 100715. 10.1016/j.xcrp.2021.100715.
50. Lim, J.W., Shin, M., Lee, D.J., Lee, S.H., and Yun, S.J. (214AD). Highly transparent amorphous silicon solar cells fabricated using thin absorber and high-bandgap-energy n/i-interface layers. *Sol. Energy Mater. Sol. Cells* **128**, 301. 10.1016/j.solmat.2014.05.041.
51. Aleo Solar GmbH (2001). Aleo Solar PV Isolierglas Isolante.
52. Mutalikdesai, A., and Ramasesha, S.K. (2017). Solution process for fabrication of thin film CdS/CdTe photovoltaic cell for building integration. *Thin Solid Films* **632**, 73–78. 10.1016/j.tsf.2017.04.036.
53. Kim, S., Yi, J., and Kim, J. (2021). Solar RRL - 2021 - Kim - Bifacial Color-Tunable Transparent Photovoltaics for Application as Building-Integrated.pdf. *Sol. RRL* **5**. 10.1002/solr.202100162.
54. Sung, Y.M., Li, M.Z., Luo, D., Li, Y. De, Biring, S., Huang, Y.C., Wang, C.K., Liu, S.W., and Wong, K.T. (2021). A micro-cavity forming electrode with high thermal stability for semi-transparent colorful organic photovoltaics exceeding 13% power conversion efficiency. *Nano Energy* **80**, 105565. 10.1016/j.nanoen.2020.105565.
55. Chen, K.S., Salinas, J.F., Yip, H.L., Huo, L., Hou, J., and Jen, A.K.Y. (2012). Semi-transparent polymer solar cells with 6% PCE, 25% average visible transmittance and a color rendering index close to 100 for power generating window applications. *Energy Environ. Sci.* **5**, 9551–9557. 10.1039/c2ee22623e.
56. Wang, C.K., Jiang, B.H., Lu, J.H., Cheng, M.T., Jeng, R.J., Lu, Y.W., Chen, C.P., and Wong, K.T. (2020). A Near-Infrared Absorption Small Molecule Acceptor for High-Performance Semitransparent and Colorful Binary and Ternary Organic Photovoltaics. *ChemSusChem* **13**, 903–913. 10.1002/cssc.201903087.
57. Hu, Z., Wang, Z., An, Q., and Zhang, F. (2020). Semitransparent polymer solar cells with 12.37% efficiency and 18.6% average visible transmittance. *Sci. Bull.* **65**, 131–137. 10.1016/j.scib.2019.09.016.
58. Li, X., Xia, R., Yan, K., Ren, J., Yip, H.L., Li, C.Z., and Chen, H. (2020). Semitransparent Organic Solar Cells with Vivid Colors. *ACS Energy Lett.* **5**, 3115–3123. 10.1021/acsenergylett.0c01554.
59. Song, W., Liu, Y., Fanady, B., Han, Y., Xie, L., Chen, Z., Yu, K., Peng, X., Zhang, X., and Ge, Z. (2021). Ultra-flexible light-permeable organic solar cells for the herbal photosynthetic growth. *Nano Energy* **86**, 106044. 10.1016/j.nanoen.2021.106044.
60. Xiao, T., Wang, J., Yang, S., Zhu, Y., Li, D., Wang, Z., Feng, S., Bu, L., Zhan, X., and Lu, G. (2020). Film-depth-dependent crystallinity for light transmission and charge transport in semitransparent organic solar cells. *J. Mater. Chem. A* **8**, 401–411. 10.1039/c9ta11613c.

61. Wageh, S., Raïssi, M., Berthelot, T., Al-Ghamdi, A.A., Abusorrah, A.M., Boukhili, W., and Al-Hartomy, O.A. (2021). Adv Eng Mater - 2021 - Wageh - Silver Nanowires Digital Printing for Inverted Flexible Semi-Transparent Solar Cells.pdf. *Adv. Eng. Mater.* **23**. 10.1002/adem.202001305.
62. Song, W., Fanady, B., Peng, R., Hong, L., Wu, L., Zhang, W., Yan, T., Wu, T., Chen, S., and Ge, Z. (2020). Foldable Semitransparent Organic Solar Cells for Photovoltaic and Photosynthesis. *Adv. Energy Mater.* **10**. 10.1002/aenm.202000136.
63. Li, Y., Guo, X., Peng, Z., Qu, B., Yan, H., Ade, H., Zhang, M., and Forrest, S.R. (2020). Color-neutral, semitransparent organic photovoltaics for power window applications. *Proc. Natl. Acad. Sci. U. S. A.* **117**, 21147–21154. 10.1073/pnas.2007799117.
64. Chang, L., Duan, L., Sheng, M., Yuan, J., Yi, H., Zou, Y., and Uddin, A. (2020). Optimising non-patterned $\text{MoO}_3/\text{Ag}/\text{MoO}_3$ anode for high-performance semi-transparent organic solar cells towards window applications. *Nanomaterials* **10**, 1–11. 10.3390/nano10091759.
65. Yao, M., Li, T., Long, Y., Shen, P., Wang, G., Li, C., Liu, J., Guo, W., Wang, Y., Shen, L., et al. (2020). Color and transparency-switchable semitransparent polymer solar cells towards smart windows. *Sci. Bull.* **65**, 217–224. 10.1016/j.scib.2019.11.002.
66. Bai, Y., Zhao, C., Chen, X., Zhang, S., Zhang, S., Hayat, T., Alsaedi, A., Tan, Z., Hou, J., and Li, Y. (2019). Interfacial engineering and optical coupling for multicolored semitransparent inverted organic photovoltaics with a record efficiency of over 12%. *J. Mater. Chem. A* **7**, 15887–15894. 10.1039/c9ta05789g.
67. Xia, R., Brabec, C.J., Yip, H.L., and Cao, Y. (2019). High-Throughput Optical Screening for Efficient Semitransparent Organic Solar Cells. *Joule* **3**, 2241–2254. 10.1016/j.joule.2019.06.016.
68. Li, Y., Ji, C., Qu, Y., Huang, X., Hou, S., Li, C.Z., Liao, L.S., Guo, L.J., and Forrest, S.R. (2019). Enhanced Light Utilization in Semitransparent Organic Photovoltaics Using an Optical Outcoupling Architecture. *Adv. Mater.* **31**, 1–8. 10.1002/adma.201903173.
69. Jose Da Silva, W., Kim, H.P., Rashid Bin Mohd Yusoff, A., and Jang, J. (2013). Transparent flexible organic solar cells with 6.87% efficiency manufactured by an all-solution process. *Nanoscale* **5**, 9324–9329. 10.1039/c3nr03011c.
70. Song, S., Cho, H.W., Jeong, J., Yoon, Y.J., Park, S.Y., Song, S., Woo, B.H., Jun, Y.C., Walker, B., and Kim, J.Y. (2020). Dichroic $\text{Sb}_2\text{O}_3/\text{Ag}/\text{Sb}_2\text{O}_3$ Electrodes for Colorful Semitransparent Organic Solar Cells. *Sol. RRL* **4**, 1–10. 10.1002/solr.202000201.
71. Corzo, D., Bihar, E., Alexandre, E.B., Rosas-Villalva, D., and Baran, D. (2021). Ink Engineering of Transport Layers for 9.5% Efficient All-Printed Semitransparent Nonfullerene Solar Cells. *Adv. Funct. Mater.* **31**, 1–10. 10.1002/adfm.202005763.
72. Liu, Q., Gerling, L.G., Bernal-Texca, F., Toudert, J., Li, T., Zhan, X., and Martorell, J. (2020). Light Harvesting at Oblique Incidence Decoupled from Transmission in Organic Solar Cells Exhibiting 9.8% Efficiency and 50% Visible Light Transparency. *Adv. Energy Mater.* **10**. 10.1002/aenm.201904196.
73. Lee, J., Cha, H., Yao, H., Hou, J., Suh, Y.H., Jeong, S., Lee, K., and Durrant, J.R. (2020). Toward Visibly Transparent Organic Photovoltaic Cells Based on a Near-Infrared Harvesting Bulk Heterojunction Blend. *ACS Appl. Mater. Interfaces* **12**, 32764–32770. 10.1021/acsami.0c08037.
74. Lunt, R.R., and Bulovic, V. (2011). Transparent, near-infrared organic photovoltaic solar cells for window and energy-scavenging applications. *Appl. Phys. Lett.* **98**. 10.1063/1.3567516.
75. Chaturvedi, N., Gasparini, N., Corzo, D., Bertrandie, J., Wehbe, N., Troughton, J., and Baran, D.

- (2021). All Slot-Die Coated Non-Fullerene Organic Solar Cells with PCE 11%. *Adv. Funct. Mater.* 31. 10.1002/adfm.202009996.
76. Chen, C.C., Dou, L., Zhu, R., Chung, C.H., Song, T. Bin, Zheng, Y.B., Hawks, S., Li, G., Weiss, P.S., and Yang, Y. (2012). Visibly transparent polymer solar cells produced by solution processing. *ACS Nano* 6, 7185–7190. 10.1021/nn3029327.
77. Yang, C., Moemeni, M., Bates, M., Sheng, W., Borhan, B., and Lunt, R.R. (2020). High-Performance Near-Infrared Harvesting Transparent Luminescent Solar Concentrators. *Adv. Opt. Mater.* 8, 1–6. 10.1002/adom.201901536.
78. Advanced Energy Materials - 2013 - Zhao - Transparent Luminescent Solar Concentrators for Large-Area Solar Windows Enabled.pdf.
79. Advanced Optical Materials - 2014 - Zhao - Near-Infrared Harvesting Transparent Luminescent Solar Concentrators.pdf.
80. López-López, C., Colodrero, S., and Míguez, H. (2014). Panchromatic porous specular back reflectors for efficient transparent dye solar cells. *Phys. Chem. Chem. Phys.* 16, 663–668. 10.1039/c3cp53939c.
81. Tagliaferro, R., Colonna, D., Brown, T.M., Reale, A., and Di Carlo, A. (2013). Interplay between transparency and efficiency in dye sensitized solar cells. *Opt. Express* 21, 3235. 10.1364/oe.21.003235.
82. Aftabuzzaman, M., Kim, C.K., Zhou, H., and Kim, H.K. (2020). In situ preparation of Ru-N-doped template-free mesoporous carbons as a transparent counter electrode for bifacial dye-sensitized solar cells. *Nanoscale* 12, 1602–1616. 10.1039/c9nr09019c.
83. Chalkias, D.A., Charalampopoulos, C., Andreopoulou, A.K., Karavioti, A., and Stathatos, E. (2021). Spectral engineering of semi-transparent dye-sensitized solar cells using new triphenylamine-based dyes and an iodine-free electrolyte for greenhouse-oriented applications. *J. Power Sources* 496, 229842. 10.1016/j.jpowsour.2021.229842.
84. Huaultmé, Q., Mwalukuku, V.M., Joly, D., Liotier, J., Kervella, Y., Maldivi, P., Narbey, S., Oswald, F., Riquelme, A.J., Anta, J.A., et al. (2020). Photochromic dye-sensitized solar cells with light-driven adjustable optical transmission and power conversion efficiency. *Nat. Energy* 5, 468–477. 10.1038/s41560-020-0624-7.
85. Cells, G.D.S., Chalkias, D.A., Charalampopoulos, C., Aivali, S., Andreopoulou, A.K., Karavioti, A., and Stathatos, E. (2021). A Di-Carbazole-Based Dye as a Potential Sensitizer for Greenhouse-Integrated Dye-Sensitized Solar Cells. *Energies* 14, 1–15.
86. Kim, K., Nam, S.K., and Moon, J.H. (2020). Dual-Band Luminescent Solar Converter-Coupled Dye-Sensitized Solar Cells for High-Performance Semitransparent Photovoltaic Device. *ACS Appl. Energy Mater.* 3, 5277–5284. 10.1021/acsaem.0c00171.
87. Naim, W., Novelli, V., Nikolinakos, I., Barbero, N., Dzeba, I., Grifoni, F., Ren, Y., Alnasser, T., Velardo, A., Borrelli, R., et al. (2021). Transparent and Colorless Dye-Sensitized Solar Cells Exceeding 75% Average Visible Transmittance. *JACS Au* 1, 409–426. 10.1021/jacsau.1c00045.
88. Tapilouw, A.M., Chang, Y.-W., Yu, L.-Y., and Wang, H.-W. (2016). Reduction of batwing effect in white light interferometry for measurement of patterned sapphire substrates (PSS) wafer. *Interferom. XVIII* 9960, 996006. 10.1117/12.2236874.